Geoscience Frontiers xxx (xxxx) xxx

Contents lists available at ScienceDirect

Geoscience Frontiers

journal homepage: www.elsevier.com/locate/gsf

Research Paper

Unraveling one billion years of geological evolution of the southeastern Amazonia Craton from detrital zircon analyses

Camille Rossignol [a,b,c,*], Paul Yves Jean Antonio [a], Francesco Narduzzi [a,c], Eric Siciliano Rego [b,c,d], Lívia Teixeira [a], Romário Almeida de Souza [e], Janaína N. Ávila [f], Marco A.L. Silva [g], Cristiano Lana [g], Ricardo I.F. Trindade [a], Pascal Philippot [a,c]

[a] Departamento de Geofísica, Instituto de Astronomia, Geofísica e Ciências Atmosféricas da Universidade de São Paulo, Rua do Matão, 1226 - Cidade Universitária, São Paulo 05508-090, Brazil
[b] Institut de Physique du Globe de Paris, Université de Paris, CNRS, Paris, France
[c] Géosciences Montpellier, Université de Montpellier, CNRS, Université des Antilles, Montpellier, France
[d] Instituto de Geociências, Universidade de São Paulo, Rua do Lago, 562 - Cidade Universitária, São Paulo 05508-080, Brazil
[e] Instituto de Geociências e Engenharias, Universidade Federal do Sul e Sudeste do Pará – UNIFESSPA, Folha 17, Quadra 04, Lote especial, Nova Marabá, Marabá, Pará 68505-080, Brazil
[f] Research School of Earth Sciences, The Australian National University, 142 Mills Road, Canberra, ACT 2601, Australia
[g] Applied Isotope Research Group, Departamento de Geologia, Escola de Minas, Universidade Federal de Ouro Preto, Rua Diogo de Vasconcelos, 122, 35400-000 Ouro Preto, MG, Brazil

ARTICLE INFO

Article history:
Received 15 November 2020
Revised 19 March 2021
Accepted 2 April 2021
Available online xxxx

Keywords:
Carajás Basin
Chemical Abrasion–LA-ICP-MS analyses
Age distribution comparison
Parauapebas Large Igneous Province
Transamazonian orogeny

ABSTRACT

Despite representing one of the largest cratons on Earth, the early geological evolution of the Amazonia Craton remains poorly known due to relatively poor exposure and because younger metamorphic and tectonic events have obscured initial information. In this study, we investigated the sedimentary archives of the Carajás Basin to unravel the early geological evolution of the southeastern Amazonia Craton. The Carajás Basin contains sedimentary rocks that were deposited throughout a long period spanning more than one billion years from the Mesoarchean to the Paleoproterozoic. The oldest archives preserved in this basin consist of a few ca. 3.6 Ga detrital zircon grains showing that the geological roots of the Amazonia Craton were already formed by the Eoarchean. During the Paleoarchean or the early Mesoarchean (<3.1 Ga), the Carajás Basin was large and rigid enough to sustain the formation and preservation of the Rio Novo Group greenstone belt. Later, during the Neoarchean, at ca. 2.7 Ga, the southeastern Amazonia Craton witnessed the emplacement of the Parauapebas Large Igneous Province (LIP) that probably covered a large part of the craton and was associated with the deposition of some of the world largest iron formations. The emplacement of this LIP immediately preceded a period of continental extension that formed a rift infilled first by iron formations followed by terrigenous sediments. This major change of sedimentary regime might have been controlled by the regional tectonic evolution of the Amazonia Craton and its emergence above sea-level. During the Paleoproterozoic, at ca. 2.1 Ga, the Rio Fresco Group, consisting of terrigenous sediments from the interior of the Amazonia Craton, was deposited in the Carajás Basin. At that time, the Amazonian lithosphere could have either underwent thermal subsidence forming a large intracratonic basin or could have been deformed by long wavelength flexures that induced the formation of basins and swells throughout the craton under the influence of the growing Transamazonian mountain belt.

1. Introduction

The Amazonia Craton (Fig. 1A) represents one of the largest cratons on Earth and occupies most of the northern part of the present-day South American continent (de Almeida et al., 2000; Cordani and Teixeira, 2007). The Amazonia Craton, subdivided into the Guyana Shield to the north and the Central Brazilian Shield to the south (Fig. 1B), comprises several tectonic provinces defined by

* Corresponding author at: Departamento de Geofísica, Instituto de Astronomia, Geofísica e Ciências Atmosféricas da Universidade de São Paulo, Rua do Matão, 1226 - Cidade Universitária, São Paulo 05508-090, Brazil.
E-mail address: camil.rossignol@gmail.com (C. Rossignol).

https://doi.org/10.1016/j.gsf.2021.101202
1674-9871/

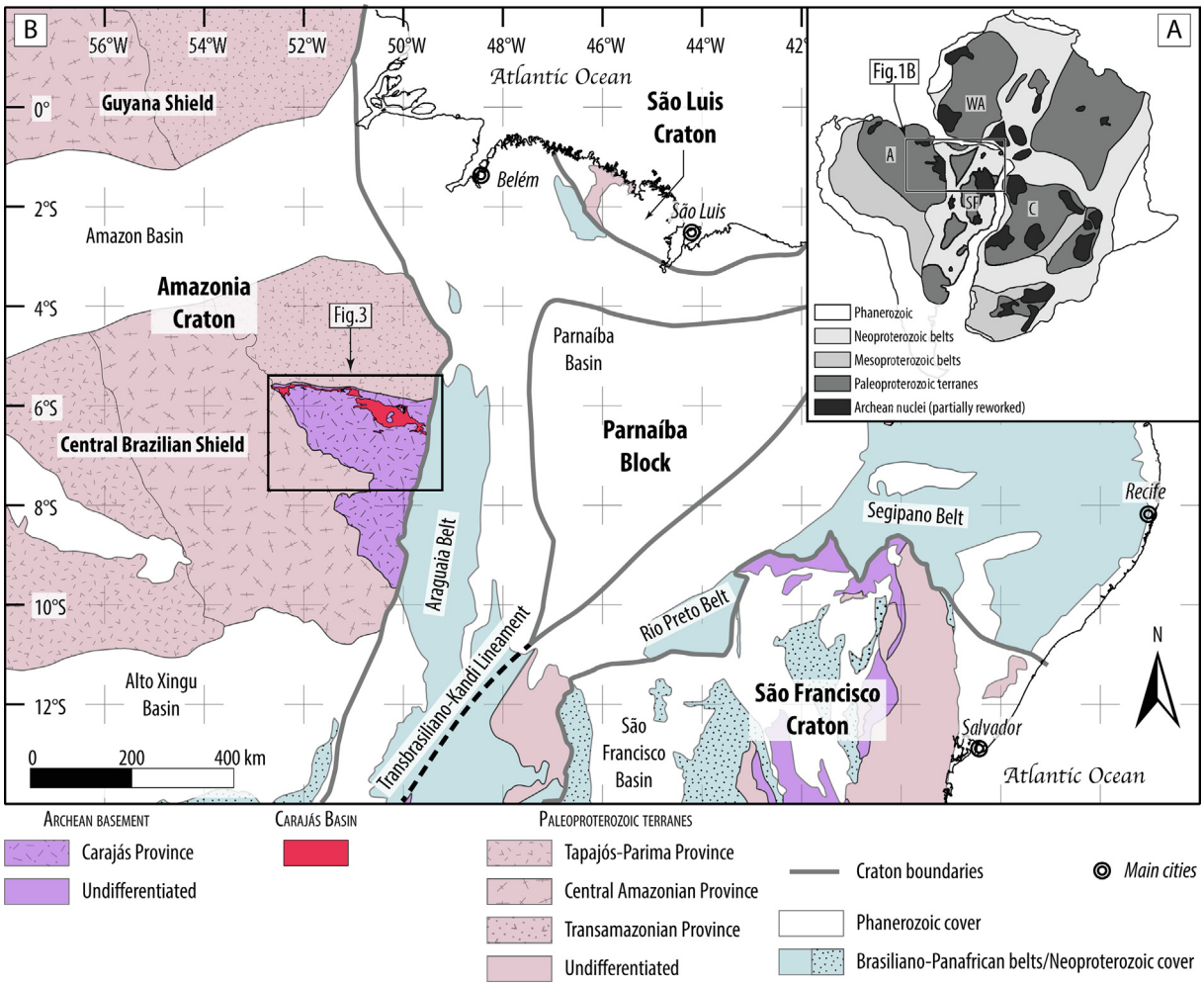

Fig. 1. Geological framework of the Amazonia Craton and the Carajás Basin. (A) Schematic West Gondwana reconstruction of the main tectonic elements of South America and Africa. Modified after Cordani et al. (2016). A: Amazonia Craton; C: Congo Craton; SF: São Francisco Craton; WA: West African Craton. (B) Location of the Carajás Basin within the Amazonia Craton (adapted after Cordani et al., 2016).

coherent structural and geochronological patterns, which correspond to different blocks that accreted together during the Proterozoic (Tassinari and Macambira, 1999; Santos et al., 2000; Cordani and Teixeira, 2007; Cordani et al., 2009). Most of the tectonic provinces that compose the Amazonia Craton are made up of Proterozoic continental crust (Santos et al., 2000; Cordani and Teixeira, 2007; Cordani et al., 2009), but locally preserve remnants of Paleoarchean and Eoarchean crust (Milhomem Neto and Lafon, 2019). The only tectonic province made up of Archean crust defines the Carajás Tectonic Province (hereafter referred to as the Carajás Province), which forms a large triangular-shaped area located to the southeast of the Amazonia Craton (Fig. 1B; Santos et al., 2000; Vasquez and Rosa-Costa, 2008).

Despite being one of the world's major metallogenic province (Cabral and Riehl, 2020; Trunfull et al., 2020), the tectonic evolution of the Carajás Province remains poorly documented. Various Meso- to Neoarchean episodes of crustal formation have been identified in the Carajás Province (Machado et al., 1991; Pidgeon et al., 2000; Almeida et al., 2013; Althoff et al., 2014), but its stabilization and the timing at which the lithosphere became rigid enough to sustain the development of sedimentary basins is not well constrained. Recent advances have allowed to better characterize the stratigraphic framework for some Neoarchean to Paleoproterozoic sedimentary units (Araujo and Nogueira, 2019; Araújo Filho et al., 2020), although the age of some sedimentary units and type of tectonic regime during basin formation remain unknown (Table 1; Fig. 2). Older sedimentary units are very poorly studied and their age, the nature of their sediments, as well as the type of basin in which they have been deposited, are also largely unknown.

In the present study, we provide new U-Pb zircon geochronological results in order to (i) better constrain the age of major sedimentary units and (ii) complement the presently available dataset of U-Pb detrital zircon ages. We then use this dataset to document the tectonic evolution of areas surrounding the Carajás Basin and reconstruct the first order geological events that occurred in the eastern Amazonia Craton between the Mesoarchean (ca. 3.2 Ga) and the Paleoproterozoic (ca. 2.1 Ga). Using the sedimentary record to document the tectonic evolution of surrounding areas is a well-established approach (Najman, 2006) and is especially suited for ancient and poorly exposed cratons such as the Amazonia Craton, where information from source regions is obscured by later metamorphism, tectonism or erosion, and for which a large dataset of U-Pb ages obtained from detrital zircon is available.

Table 1
Summary of age constraints for the main sedimentary units of the Carajás Basin.

Number in Fig. 2	Method	Object	Interpretation	Age (Ma)	Reference
Rio Novo Group					
1	Zircon U-Pb	Gabbro intruding the Rio Novo Group	Minimum depositional age	2763 ± 6	Machado et al., 1991
Parauapebas Formation					
2	Zircon U-Pb	Metarhyolite	Depositional age	2759 ± 2	Machado et al., 1991
3	Zircon U-Pb	Metabasalt	Depositional age	2750 ± 7	Martins et al., 2017
Carajás Formation					
4	Zircon U-Pb	Dolerite sill intruding the Carajás Formation	Minimum depositional age	2751 ± 4	Krymsky et al., 2007
5	Zircon U-Pb	Volcaniclastic layer	Depositional age	2720 ± 6	Rossignol et al., submitted
Igarapé Bahia Group					
6	Zircon U-Pb	Sandstones to conglomerates	Maximum depositional age	2684 ± 10	Rossignol et al., 2020a
7	Monazite U-Pb	Hydrothermal vein	Minimum depositional age	2575 ± 12	Tallarico et al., 2005
Águas Claras Formation					
8	Zircon U-Pb	Sandstone	Depositional age	2681 ± 5	Trendall et al., 1998
9	Zircon U-Pb	Granite intruding the Águas Claras Formation	Minimum depositional age	1880 ± 2	Machado et al., 1991

Uncertainties are given at the 2σ level.

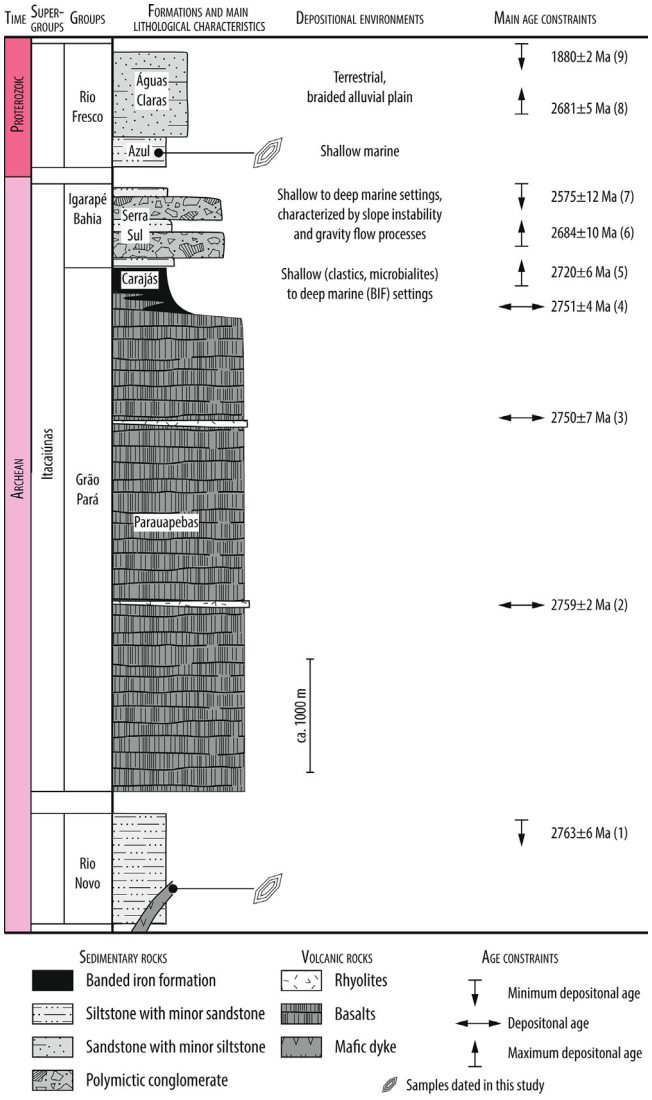

Fig. 2. Main sedimentary units of the Carajás Basin. Stratigraphic column adapted after Araújo Filho et al. (2020); Araujo and Nogueira (2019); Klein and Ladeira (2002); Machado et al. (1991); Trendall et al. (1998). References for age constraints are given in Table 1.

2. Geological setting

2.1. Regional context

The Carajás Province is classically subdivided in two structural domains delimited by the Canãa dos Carajás Shear Zone (Fig. 3) referred to as the Carajás Domain to the north and the Rio Maria Domain to the south (Vasquez et al., 2008). The Carajás Domain hosts the Carajás Basin, which is an elongated, E–W trending basin, delineated by the Cinzento Strike-Slip System to the north and by the Canaã dos Carajás Shear Zone to the south (Fig. 3). To the east, the Carajás Basin is delimited by major thrusts of the Neoproterozoic Araguaia Belt (Fig. 3A). To the west, the Carajás Basin is covered by the ca. 1.9 Ga Uatumã Silicic Large Igneous Province (SLIP; Machado et al., 1991; Dall'Agnol et al., 2005; Roverato, 2016; Silva et al., 2016; Antonio et al., 2017, 2021; Teixeira et al., 2019). The present-day fault boundaries do not reflect the initial geometry of the basin but rather correspond to major shear zones which had protracted movement histories during the Mesoarchean which were reactivated during the Paleoproterozoic (Pinheiro and Holdsworth, 1997; Tavares et al., 2018).

The basement of the Carajás Basin is heterogeneous and includes various Meso- to Neoarchean rocks (Tavares et al., 2018; Vasquez and Rosa-Costa, 2008) that formed during successive magmatic events that lasted between ~ 20 Myr and ~ 150 Myr (Feio et al., 2013; Trunfull et al., 2020). The oldest basement rocks consist of metamorphic rocks with protolith ages of ca. 3080 Ma to ca. 3000 Ma (Machado et al., 1991; Pidgeon et al., 2000; Moreto et al., 2015). A second magmatic event linked to the emplacement of tonalites, trondhjemites and granodiorites (TTG) occurred between ca. 2960 Ma and ca. 2930 Ma (Feio et al., 2013). A younger episode of TTG magmatism occurred between ca. 2870 Ma to 2830 Ma (Feio et al., 2013; Machado et al., 1991; Moreto et al., 2015; Pidgeon et al., 2000). The basement was then intruded by a variety of ultramafic and mafic bodies and A-type granitoids mainly emplaced between ca. 2760 Ma and ca. 2730 Ma (Barros et al., 2009; Feio et al., 2012, 2013; Machado et al., 1991; Sardinha et al., 2006). This magmatic event was likely responsible for the eruption of basalts at 2774 ± 19 Ma in the north of the Carajás Domain (Toledo et al., 2019). A minor magmatic event later affected the Carajás Domain at 2701 ± 30 Ma (Melo et al., 2017). A final tectono-thermal event occurred between ca. 2600 Ma and 2450 Ma (Machado et al., 1991; Requia et al., 2003; Tallarico et al., 2005; Grainger et al., 2008; Melo et al., 2017; Toledo et al., 2019). This episode remains poorly constrained and is mainly documented by metamorphic ages ranging from 2584 ± 4 Ma (titanite U-Pb age in a granitoid; Machado et al., 1991) to 2555 ± 4 Ma and

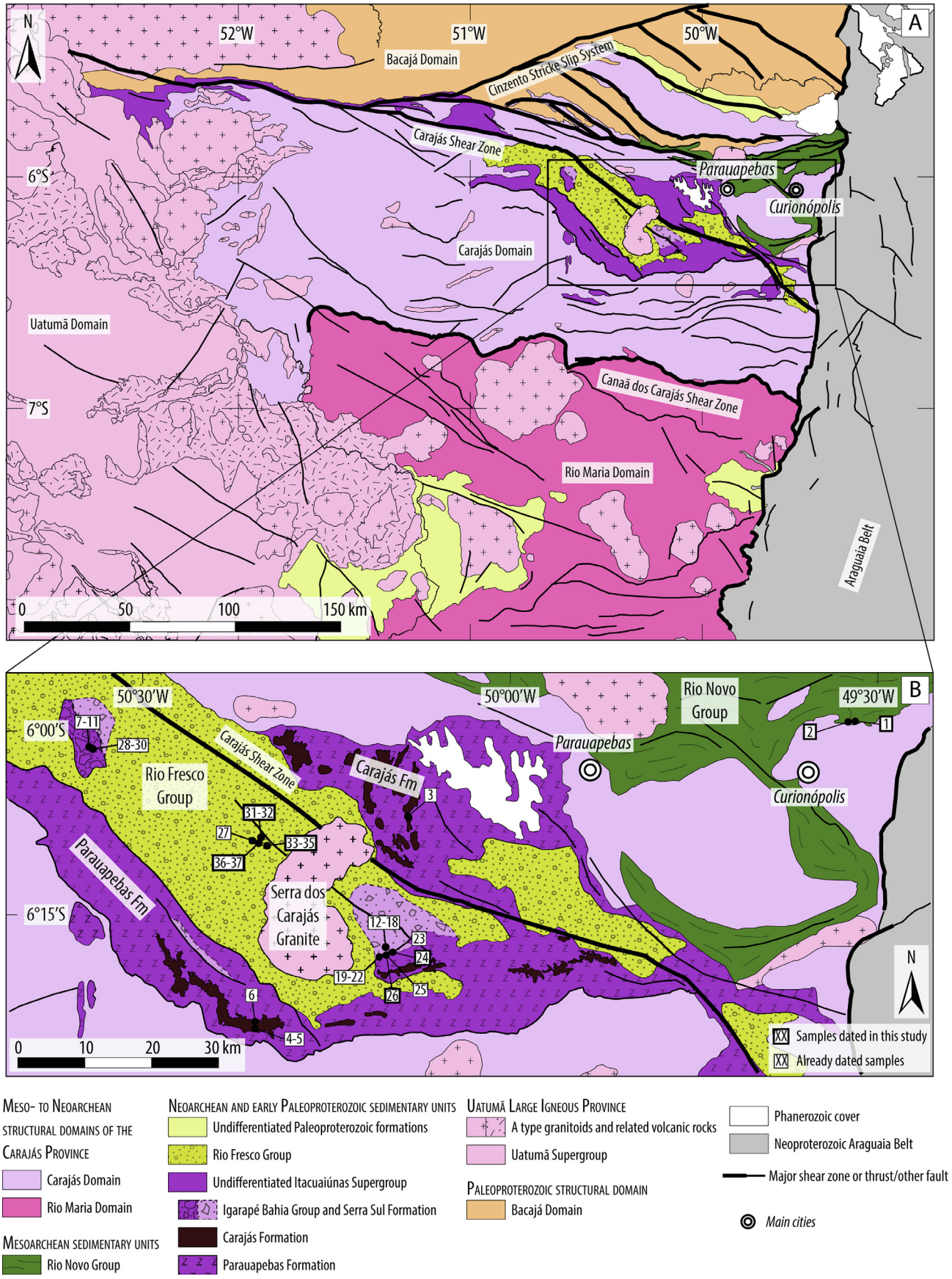

Fig. 3. Geological map of the Carajás Basin. (A) Geological map of the Carajás Basin (after Vasquez et al., 2008). See Fig. 1 for regional context. (B) Location of the samples used in this study. Mapping of the Serra Sul Formation modified after Araújo Filho et al. (2020). Numbers refers to Tables 2 and 3. Coordinates of the samples are available in the Appendix 1.

2551 ± 2 Ma (zircon U-Pb and monazite U-Pb in amphibolite and metamorphic iron formation, respectively; Machado et al., 1991). This metamorphic event was accompanied by intense hydrothermal circulations dated by hydrothermal monazite with U-Pb ages ranging from 2575 ± 12 Ma (Tallarico et al., 2005) to 2452 ± 14 Ma (Melo et al., 2017) and sulfide minerals dated by Re-Os at 2576 ± 8 Ma and 2568 ± 8 Ma (Requia et al., 2003). Small bodies of granitic rocks and pegmatites emplaced at 2557 ± 26 Ma and 2562 ± 39 Ma, respectively (U-Pb zircon age) were also produced during this long-lasting event (Toledo et al., 2019).

To the south of the Carajás Domain, the Rio Maria Domain (Fig. 3A) comprises Mesoarchean greenstone belts with komatiites (Siepierski and Ferreira Filho, 2016) and TTG emplaced between ca. 2980 Ma and ca. 2920 Ma (Almeida et al., 2013). A second magmatic episode, characterized by TTG and sanukitoid suites, occurred between ca. 2870 Ma and ca. 2860 Ma (Almeida et al., 2013; Althoff et al., 2014; Feio et al., 2013; Macambira and Lancelot, 1996). Tavares et al. (2018) suggested that the Rio Maria Domain has been accreted onto the Carajás Domain during the end of the Mesoarchean, between ca. 2.87 Ga and ca. 2.83 Ga.

To the north of the Carajás Domain, the Bacajá Domain (Fig. 3A) comprises various metamorphic and magmatic rocks (Vasquez et al., 2008). The basement of the Bacajá Domain consists of ca. 2670 Ma tonalites and greenstone belts with metavolcanics rocks emplaced between ca. 2360 Ma and ca. 2340 Ma (Macambira et al., 2009). The Bacajá Domain was latter intruded by a series of Rhyacian granitoids during a time interval of ~ 140 Myr, from ca. 2220 Ma to ca. 2080 Ma (Macambira et al., 2009). The age of the welding of the Bacajá and Carajás domains is debated. A collision of these two domains at ca. 2.1 Ga has been proposed, based on the interpretation that Rhyacian granitoids formed along a subduction zone where oceanic lithosphere attached to the Carajás Domain subducted beneath the Bacajá Domain (Macambira et al., 2009; Tavares et al., 2018). On the contrary, geophysical and geochronological data suggests that the Bacajá and Carajás domains shared a similar Archean geological evolution, which would imply an older Archean collision (Motta et al., 2019). Irrespective of the age of the collision between the Carajás and Bacajá domains, the latter has been extensively reworked during the Transamazonian orogeny (Macambira et al., 2009; Tavares et al., 2018; Motta et al., 2019). The Bacajá Domain thus represents a segment of a major orogen that extended from northern South America (Hurley et al., 1967; Santos et al., 2000) to the southern part of the São Francisco Craton (Teixeira and Figueiredo, 1991; Machado et al., 1996; Alkmim and Marshak, 1998; Cutts et al., 2018; Moreira et al., 2018) and the Western Africa and Congo cratons (Bertrand and Jardim de Sa, 1990; Schofield et al., 2006; Baratoux et al., 2011; Parra-Avila et al., 2019), where the orogen is referred to as Eburnean (Hurley et al., 1967).

To the east, the Carajás Domain is bounded by the Neoproterozoic Araguaia Belt (Fig. 3A). This fold and thrust belt correspond to a segment of the Brasiliano orogen (de Almeida et al., 2000). The emplacement of doleritic dykes at ca. 535 Ma in the Carajás Domain is attributed to the late to post-orogenic extension of the Brasiliano orogen (Teixeira et al., 2019).

During the Phanerozoic, the Carajás Domain remained relatively stable. Nonetheless, it has been affected by a magmatic event during the Triassic-Jurassic transition (ca. 200 Ma) characterized by mafic dykes of the Central Atlantic Magmatic Province (Teixeira et al., 2019). During the Cretaceous (ca. 75 Ma), major faults were reactivated and hydrothermal activity affected the Carajás Domain, probably as the result of far field effects of the opening of the South Atlantic Ocean (Cabral et al., 2011).

2.2. Sedimentological framework of the sedimentary series from the Carajás Basin

The stratigraphic subdivision of the Carajás Basin is outlined in Fig. 2. The oldest unit consists of the Rio Novo Group, which is unconformably overlain by the Itacaiúnas Supergroup, subdivided into the Grão Pará and the Igarapé Bahia groups. The Rio Novo Group and Itacaiúnas Supergroup experienced moderate to high grade metamorphic conditions, from upper greenschist to upper amphibolite facies (Araujo and Maia, 1991; Machado et al., 1991; Pinheiro and Holdsworth, 1997; Tavares et al., 2018). For simplicity, the prefix "meta-" has been omitted in the following presentation of sedimentary rocks. The Rio Fresco Group, which unconformably overlain older sedimentary units, remained unmetamorphosed or has experienced only low grade-metamorphism overprint (Pinheiro and Holdsworth, 1997; Araújo Filho et al., 2020).

2.2.1. Rio Novo Group

This sedimentary unit is exposed only to the north Carajás Shear Zone, in the northeastern part of the Carajás Domain (Fig. 3). The Rio Novo Group is mainly made up of pelites interbedded with subordinate iron formations, cherts, arenites, conglomerates and volcanic rocks (Fig. 2; Hirata et al., 1982; Araujo and Maia, 1991). This sedimentary association has been interpreted to represent a greenstone belt sequence (Hirata et al., 1982; Grainger et al., 2008; Tavares et al., 2018).

The Rio Novo Group experienced multiple deformation events, greenschist facies metamorphism (Hirata et al., 1982), and local, yet intense, hydrothermal alteration (Berni et al., 2014). Although poorly dated, the Rio Novo Group represents one of the oldest sedimentary units of the Carajás Basin and is generally assumed to be early Neoarchean or Mesoarchean in age (Vasquez et al., 2008). An age constraint is given by the Luanga magmatic complex that intruded the Rio Novo Group at 2763 ± 6 Ma (Table 1, Fig. 2).

2.2.2. Itacaiúnas Supergroup

This unit consists of volcanic, volcaniclastic, and terrigenous rocks as well as iron formations exposed over >300 km along the E–W strike of the Carajás Basin (Fig. 3). The Itacaiúnas Supergroup is subdivided into the Grão Pará Group at the base and the Igarapé Bahia Group at the top (Fig. 2).

The Grão Pará Group comprises the Parauapebas and the Carajás formations. The former consists of basalts, basaltic andesites but also minor pyroclastic rocks and rhyolites (Dardenne et al., 1988; Teixeira and Eggler, 1994; Martins et al., 2017). The age of the Parauapebas Formation is well constrained to between ca. 2770 Ma and ca. 2750 Ma (Table 1, Fig. 2), as indicated by numerous U-Pb analyses on volcanic zircon grains (Wirth et al., 1986; Olszewski et al., 1989; Machado et al., 1991; Trendall et al., 1998; Martins et al., 2017). The Parauapebas Formation is conformably overlain by the Carajás Formation (Gibbs et al., 1986; Martins et al., 2017; Fig. 2). This formation is mainly made up of banded iron formations (Tolbert et al., 1971; Klein and Ladeira, 2002; Dalstra and Guedes, 2004) but also comprises minor black shales (Cabral et al., 2017) and conglomerates (Cabral et al., 2013). Banded Iron Formation (BIF) sometimes contain biogenic features (Ribeiro da Luz and Crowley, 2012). The depositional environments of the Carajás Formation range from shallow to deep water settings (Lindenmayer et al., 2001; Ribeiro da Luz and Crowley, 2012). The age of the Carajás Formation is well constrained between 2743 ± 11 Ma and 2720 ± 6 Ma (Table 1, Fig. 2; Trendall et al., 1998).

The tectonic setting of the Carajás Basin attending the deposition of the Grão Pará Group is controversial. Possible models include a greenstone belt (Figueiredo e Silva et al., 2008), continen-

tal rift (Olszewski et al., 1989; Feio et al., 2012; Tavares et al., 2018; Toledo et al., 2019), possibly related to post-orogenic extension (Martins et al., 2017; Tavares et al., 2018), pull-apart (Teixeira and Eggler, 1994) or back-arc basin (Dardenne et al., 1988). In addition, the emplacement of A-type granitoids coeval with Parauapebas volcanism has been suggested to have occurred in a collisional setting (Barros et al., 2009; Dall'Agnol et al., 2017).

The Igarapé Bahia Group (Fig. 2) forms the uppermost unit of the Itacaiúnas Supergroup. Recently, Araujo and Nogueira (2019) have defined a new subdivision of the Itacaiúnas Supergroup named the Serra Sul Formation. The Serra Sul Formation has sedimentological and deformation patterns that are essentially similar to those of the Igarapé Bahia Group, and both sedimentary units are coeval (Melo et al., 2019; Rossignol et al., 2020a). In the present work, the Serra Sul Formation is thus included into the Igarapé Bahia Group (Fig. 2). This group is made up of polymictic conglomerates with angular clasts of BIF, cherts, volcanic and metamorphic rocks that are interbedded with fine-grained sediments (Ronze et al., 2000; Dreher et al., 2005, 2008; Galarza et al., 2008; Araujo and Nogueira, 2019; Melo et al., 2019; Rossignol et al., 2020a). Flat pebble conglomerates and microbialites are also common (Rossignol et al., 2020a). Toward its base, the Igarapé Bahia Group contains BIF layers up to 10 m thick similar to those of the underlying Carajás Formation (Melo et al., 2019). The different sedimentary features of the Igarapé Bahia Group point toward various subaqueous depositional environments, ranging from shallow to deep water settings influenced by slope instability and gravity flow processes (Dreher et al., 2005, 2008; Rossignol et al., 2020a). The Igarapé Bahia Group experienced greenschist facies metamorphism (Villas and Santos, 2001; Tallarico et al., 2005; Galarza et al., 2008) and has been locally affected by intense fluid circulation (Ronze et al., 2000; Villas and Santos, 2001; Dreher et al., 2005, 2008; Tallarico et al., 2005; Galarza et al., 2008). The age of the Igarapé Bahia Group is constrained between 2684 ± 10 Ma and 2575 ± 12 Ma (Tallarico et al., 2005; Table 1, Fig. 2).

The tectonic setting of the Carajás Basin at the time of deposition of the Igarapé Bahia Group is as controversial as those proposed for the deposition of the Grão Pará Group. Most studies postulate that the tectonic regime remained unchanged during the deposition of the Grão Pará and Igarapé Bahia groups, so that controversies about tectonic setting for the Grão Pará Group also applies for the Igarapé Bahia Group (Olszewski et al., 1989; Teixeira and Eggler, 1994; Feio et al., 2012; Tavares et al., 2018; Toledo et al., 2019). Others have argued that the Igarapé Bahia Group represents a volcanic arc associated with a subduction zone, whereas the Grão Pará Group formed in a back-arc setting (Dardenne et al., 1988; Melo et al., 2019).

2.2.3. Rio Fresco Group

The Rio Fresco Group (Fig. 2; Machado et al., 1991; Trendall et al., 1998) comprises the Azul Formation (Araújo Filho et al., 2020) and the Águas Claras Formation (Dreher et al., 2005, 2008; Galarza et al., 2008). The Azul Formation is made up of mudstone, siltstone and sandstone that have been deformed and experienced low-grade metamorphism (Araújo Filho et al., 2020). These sediments are interpreted to have been deposited in a marine platform (Araújo Filho et al., 2020).

The Águas Claras Formation consists of sandstones and siltstones with minor conglomerates (Araujo and Maia, 1991; Melo et al., 2019) deposited in a braided fluvial plain (Araujo and Maia, 1991; Araújo Filho et al., 2020). Paleocurrent reconstruction suggests that the rivers flowed towards the west (present day coordinates; Araujo and Maia, 1991). The age of the Rio Fresco Group is poorly defined (Table 1) and occurred in a large time interval ranging between 2681 ± 5 Ma and 1880 ± 2 Ma (Table 1; Machado et al., 1991; Trendall et al., 1998).

The tectonic setting of the Carajás Basin at the time of deposition of the Rio Fresco Group is debated. A transtensional setting associated with shear zone activity and forming a pull apart basin has been proposed (Teixeira and Eggler, 1994; Melo et al., 2019). Alternatively, the Rio Fresco Group is suggested to have been deposited in a foreland basin associated with the Transamazonian orogen (Tavares et al., 2018; Araújo Filho et al., 2020).

3. Methodology

3.1. Rationale, dataset compilation and additional samples

Age distributions obtained from U-Pb analyses on detrital zircon grains can provide a record of hinterland bedrocks. Although such an approach is biased by variable concentration of zircon in bedrocks, differential erosion rates in source regions and hydrodynamic fractionation of zircon grains during transport (Amidon et al., 2005; Lawrence et al., 2011), zircon U-Pb age distributions can provide information about the tectonic setting of a basin (Fedo et al., 2003; Cawood et al., 2012; Gehrels, 2014). To investigate the Mesoarchean to Paleoproterozoic evolution of the eastern Amazonia Craton, we thus compiled all published detrital zircon U-Pb dates from Paleoproterozoic and older sediments of the Carajás Basin (Table 2, Fig. 3B, Appendix 1). Because inferring the tectonic setting from detrital zircon age distributions require (i) defining the depositional age of the investigated sedimentary unit (Cawood et al., 2012), and (ii) datasets that are large enough to ensure robust statistical analyses (Pullen et al., 2014), we collected additional samples to better constrain the age and expand the currently available detrital zircon dataset.

As the age of the Rio Novo Group is poorly defined, we collected two samples in dykes crosscutting this sedimentary units to provide a minimum depositional age for this sedimentary unit. As no detrital zircon grains from this unit have been dated, we did not carry further geochronological investigation on detrital zircon. Subsequent inferences on the tectonic setting of the Rio Novo Group thus rely on qualitative observations.

To expand the existing U-Pb detrital zircon dataset for the Rio Fresco Group, seven samples were collected on three drill cores intersecting the Azul Formation (Table 2; Fig. 3B). Different stratigraphic levels, consisting of fine- to medium-grained sandstone, have been sampled to capture potential variability in sedimentary sources and minimize biases related to sediment transport mechanisms (Hietpas et al., 2011; Lawrence et al., 2011).

3.2. U-Pb zircon geochronology

3.2.1. Analytical methods

The zircon grains were extracted following a classical mineral separation procedure and were handpicked under a binocular microscope with the aim to avoid intentional bias, even if some bias can be introduced by hand picking (Košler et al., 2013; Markwitz and Kirkland, 2018). We dated zircon grains collected in mafic dykes and in the Azul Formation following a classical procedure (e.g., Košler and Sylvester, 2003) by Laser Ablation–Inductively Coupled Plasma–Mass Spectrometry (LA-ICP-MS). Because preliminary results revealed that most of the zircon grains collected from the Igarapé Bahia Group and Azul Formation are highly discordant, we implemented a thermal annealing – chemical abrasion (TACA) procedure to treat the grains from three samples (GT12 56.00–56.20, FD02 118.80–119.15 and DH01 184.70–185.00) before analysis by LA-ICP-MS. This procedure aims to dissolve the parts of the grains where radiation damage and most likely Pb loss occurred, while keeping undissolved the crystalline, supposedly concordant, part of the grains (Crowley et al., 2014;

Table 2
Samples used in this study along with maximum depositional ages and detection limits.

Number in Fig. 3	N_{zrc}	Probability of concordance ≥ 10%, decay constants errors included									Reference
		Detection limits (%)				Maximum depositional age					
		$DL_{1(pL=0.5)}$	$DL_{1(pL=0.95)}$	$DL_{3(pL=0.5)}$	$DL_{1(pL=0.95)}$	Concordia age	± (2σ)	n	MSWD	Probability	
Carajás Formation (233 concordant grains)											
3	93	0.7	3.2	2.9	6.7	**2719.6**	**5.6**	**35**	0.47	1.00	Rossignol et al., submitted
4	67	1.0	4.4	4	9.1	2732.4	5.2	37	0.53	1.00	Rossignol et al., submitted
5	72	1.0	4.1	3.7	8.5	2728.5	5.2	38	0.57	1.00	Rossignol et al., submitted
6	1	50.0	95.0	na	na	2749	20	2	0.39	0.76	Rossignol et al., submitted
Igarapé Bahia Group (598 concordant grains)											
7	23	3.0	12.2	11.5	25	2865	25	5	0.85	0.57	Melo et al., 2019
8	11	6.3	23.8	23.6	47.1	2785	16	3	1.8	0.11	Rossignol et al., submitted
9	11	6.3	23.8	23.6	47.1	2753	18	3	0.44	0.82	Rossignol et al., submitted
10	25	2.7	11.3	10.6	23.2	2829	17	3	0.48	0.79	Rossignol et al., submitted
11	19	3.6	14.6	13.9	29.6	2788	12	6	1.1	0.36	Rossignol et al., submitted
12	77	0.9	3.8	3.5	8	2815.8	8.8	10	1.4	0.12	Rossignol et al., 2020a
13	22	3.1	12.7	12	26	2748	12	5	0.65	0.75	Rossignol et al., 2020a
14	52	1.3	5.6	5.2	11.7	2708	11	10	0.67	0.85	Rossignol et al., 2020a
15	22	3.1	12.7	12	26	2767	14	4	0.94	0.47	Rossignol et al., 2020a
16	67	1.0	4.4	4	9.1	2718	12	7	0.95	0.50	Rossignol et al., 2020a
17	33	2.1	8.7	8.1	17.9	2786	12	5	1.5	0.13	Rossignol et al., 2020a
18	75	0.9	3.9	3.6	8.2	2770.1	8.9	10	0.67	0.85	Rossignol et al., 2020a
19	11	6.3	23.8	23.6	47.1	2706	12	8	0.61	0.87	Rossignol et al., 2020a
20	2	29.3	77.6	na	na	*2947*	*23*	*2*	*0.34*	*0.80*	Rossignol et al., 2020a
21	54	1.3	5.4	5	11.3	2701.6	9.2	10	0.4	0.99	Rossignol et al., 2020a
22	32	2.1	8.9	8.3	18.4	**2674**	**17**	**4**	1.5	0.17	Rossignol et al., 2020a
23	12	5.6	22.1	21.7	43.9	2821.3	9.3	9	0.76	0.74	Rossignol et al., 2020a
24	32	2.1	8.9	8.3	18.4	2762.6	8.7	11	0.32	1.00	This work
25	13	5.2	20.6	20.1	41.1	2722.8	8.3	14	0.58	0.96	Rossignol et al., 2020a
26	5	12.9	45.1	50	81.1	2705	16	3	2.1	0.07	This work
Rio Fresco Group (202 concordant grains)											
27	18	3.8	15.3	14.6	31.1	2677.1	8.6	16	0.67	0.93	Trendall et al., 1998
28	25	2.7	11.3	10.6	23.2	2878	16	10	0.73	0.79	Melo et al., 2019
29	13	5.2	20.6	20.1	41.1	2915	22	10	1.05	0.39	Melo et al., 2019
30	9	7.4	28.3	28.7	55	2756	13	4	0.87	0.53	Rossignol et al., submitted
31	29	2.4	9.8	9.2	20.2	2819	11	10	0.92	0.55	This work
32	72	1.0	4.1	3.7	8.5	2723	16	3	1.3	0.25	This work
33	19	3.6	14.6	13.9	29.6	2908	12	8	0.94	0.52	This work
34	6	10.9	39.3	42.2	72.9	2884	17	4	1.2	0.28	This work
35	2	29.3	77.6	na	na	*2880.2*	*30.9*	*1*	*0.14*	*0.71*	This work
36	4	15.9	52.7	61.5	90.3	*2815*	*20*	*2*	*1.2*	*0.31*	This work
37	5	12.9	45.1	50	81.1	**2686**	**18**	**3**	**1.7**	**0.14**	This work

N_{zrc}: number of concordant zircon grain analyzed per sample; n: number of analyses used to calculate the maximum deposition age; DL: Detcetion Limit, that is the relative proportions of zircon population expressed as the percentage of the total population likely to remain undetected at a given confidence level (Andersen, 2005); DL_1: detection limit for at least one grain, calculated after (Andersen, 2005); DL_3: detection limit for at least three grains, calculated after Rossignol et al. (2016); $_{pL}$: probability level assigned to the detection limits; MSWD: mean square of weighted deviates. The MSWD and the probability given for the concordia ages are for both concordance and equivalence. na: non applicable.
Bold: youngest maximum depositional age of the sedimentary unit. *Italic*: maximum depositional ages not fulfilling the 3 grains criterion.

von Quadt et al., 2014; Huyskens et al., 2016). Thermal annealing was performed in ceramic crucibles at 850 °C for 60 h. After cooling, the grains were transferred into Savillex Teflon vials for partial dissolution ("chemical abrasion") into a 0.8 mL concentrated hydrofluoric acid (50% HF) and 3.6 mL 1:1 8 M HNO_3 + H_2O solution. Dissolution was performed using a Milestone bench-top Ultra-wave single reaction chamber microwave digestion system. Internal chamber conditions were set for 10 min at 175 °C, followed by a second 10 min step at 60 °C. The zircon grains were cleaned through rinsing with 4 M HCl solution then by repeated rinsing with distilled water and evaporated to dryness, mounted in resin pucks.

After embedding the grains in an epoxy resin, the pucks were hand grounded to reveal equatorial cross sections. Laser microsampling sites were chosen based on cathodoluminescence (CL) imaging by Scanning Electron Microscopy (SEM) using a JEOL 6510 equipped with a Centaurus cathodoluminescence detector. To conduct *in situ* isotopic analyses, samples were ablated using a Photon machine G2 Excimer laser system connected to a ThermoFisher Scientific Element II Sector Field-Inductively Coupled Plasma-Mass Spectrometer. During the course of the analyses, the signals of ^{204}(Pb + Hg), ^{206}Pb, ^{207}Pb, ^{208}Pb, and ^{238}U masses were acquired. No common Pb correction was applied. The ^{235}U signal was calculated from ^{238}U using the ratio $^{235}U/^{238}U = 137.88$. Laser spot diameters of 25 μm to 30 μm with repetition rates of 10 Hz were used for ablation. Analyses were performed during two analytical sessions, and BB (Santos et al., 2017) and GJ-1 (Jackson et al., 2004) standards were used as primary reference materials during analytical sessions 1 and 2, respectively, to correct for mass fractionation. BB (Santos et al., 2017), GJ-1 (Jackson et al., 2004) and Plesovice (Sláma et al., 2008) standards were used as secondary reference material to control data reproducibility. A total of 1014 U-Pb analyses were obtained on 991 detrital zircon grains, with a minimum of 10, and a maximum of 398 grains analyzed per sample, according to zircon availability. For mafic dykes, a total of 61 analyses (59 grains) were obtained. Detailed analytical methods are presented in Appendix 2.

3.2.2. Data filtering and maximum age calculations

For magmatic rocks (dykes) comprising cogenetic zircon grains, the approach consisted of calculating the upper intercept of the unforced discordia passing through the analyses. To regress the

data for upper intercept date calculation, the points were weighted proportionally to the inverse square of their errors ("model 1" regression in Isoplot; Ludwig, 2012).

For zircon grains collected in metasedimentary rocks, a two-step procedure has been applied to calculate maximum depositional ages. The first step consisted of filtering the data based on their probability of concordance calculated using the "Concordia" function in Isoplot/Ex 3.00 (decay constant errors included; Ludwig, 1998, 2012). The cut-off level applied to filter the data was 10%. In what follows, concordant analyses are those showing a probability of concordance $\geq$ 10% (Rossignol et al., 2016). Concordant analyses were then selected to calculate the maximum depositional age for each sample. To calculate maximum depositional ages (MDA), we selected the youngest cluster of at least three grains overlapping at 2σ (standard deviation) (Dickinson and Gehrels, 2009; Coutts et al., 2019). Despite such an approach can be affected by analyses from grains that suffered small Pb loss that would not have been dismissed by the concordance filter (Spencer et al., 2016), this methodology relying on at least three grains selected after applying a conservative concordance filter minimizes the risk to obtain MDA younger than the true depositional age (Dickinson and Gehrels, 2009; Coutts et al., 2019). MDA were calculated as the concordia age (Ludwig, 1998) of these youngest clusters using Isoplot/Ex 3.00 and are provided with 95% confidence limits. Hereafter quoted dates are concordia ages.

3.3. Statistical analyses of age distributions

To identify discrete age components and quantify their relative contributions and width in age distributions, we performed mixture modeling using the *Bayes Mix* software (Jasra et al., 2006). Such a procedure avoids subjective bias that affects visual interpretation of complex age distributions. *Bayes Mix* uses a Reversible Jump Markov Chain Monte Carlo (RJ-MC-MC) approach, which is an iterative, Bayesian sampling strategy that allows the number of individual components, their age, width and relative contribution to change in order to best fit a given age distribution (Jasra et al., 2006; Gallagher et al., 2009; Compston and Gallagher, 2012). After exploratory runs to determine the most probable number of components in each age distribution, we chose the expected model (Compston and Gallagher, 2012), given a specified number of components, under the assumption of normal (Gaussian) distributions. For each dataset, *Bayes Mix* was run for 10^6 iterations after 5×10^5 burn-in iterations, with a thinning factor of 10, resulting in 10^5 modeled samples used to make inferences about the number of components, age, width and their relative contribution. To account for the known duration of the different tectono-magmatic events that built the basement of the Carajás Basin that lasted up to 150 Myr (Melo et al., 2017; Toledo et al., 2019; Trunfull et al., 2020) and period of mantle differentiation events that lasted ~ 300 Myr (Feio et al., 2013; Santos et al., 2000), we set the range of acceptable value of the standard deviation for a given component to a maximum of 150 Myr (i.e., to allow the model to look for age components up to 300 Ma in width). Distribution parameters were adjusted for each run to keep the acceptance rates between 0.3 and 0.6 (Appendix 3).

In order to accurately constrain the characteristics (age, relative contributions and width) and number of discrete components in a detrital zircon population, large datasets (several hundred to thousands of individual dates) are necessary (Pullen et al., 2014; Licht et al., 2016). In the present study, datasets ranging from 202 to 598 individual dates have been used for modelling. The accuracy of discrete components characterization depends of the actual number of components in an age distribution (Pullen et al., 2014; Licht et al., 2016), and will be discussed together with the interpretation of mixture modelling results.

4. Results

4.1. Rio Novo Group

4.1.1. Field observations

The studied localities consist of an abandoned gold mine pits (Cutia mine) located to the NE of the city of Curionópolis (Fig. 3; coordinates of studied sites are available in Appendix 1). Two main lithologies were identified in the Rio Novo Group. The main lithology consists of thick and monotonous pelitic series showing a weak metamorphic cleavage (Fig. 4A, B, C). The second lithology consists of normally graded conglomerates alternating with sandstones and siltstones. The clasts, up to tens of centimeters large, are made up of quartz, mafic rocks and metapelites and exhibit rounded to angular shapes and are sometimes imbricated (Fig. 4C). Because of pervasive weathering and deformation, no sedimentary facies analysis has been undertaken. The pelites from the Rio Novo Group rocks are crosscut by numerous quartz veins, indicating channelized fluid circulation on a local scale. Both metapelites and conglomerates are intruded by mafic dykes (Fig. 4A, B, C), which have been sampled for dating purpose. The mafic dykes are made up of dolerite and sometimes show a brecciated texture with quartz veins comprising native gold.

4.1.2. Geochronological results

Cathodoluminescence (CL) images of representative grains are presented in Fig. 5, and the geochronological results are presented in Fig. 6. Analytical results are available in Appendix 4.

Sample PC01. This dolerite contains numerous small slightly pinkish zircon grains displaying euhedral and prismatic shapes (2:1 length to width ratio). In CL, the grains display a well-defined oscillatory zoning (Fig. 5A) typical of magmatic zircon (e.g., Shore and Fowler, 1996; Corfu et al., 2003). The zircon Th/U ratios range between 0.15 and 3.18, also supporting a magmatic origin (e.g., Rubatto, 2002).

Among 54 grains analyzed, 47 datapoints align in a $^{206}Pb/^{238}U$–$^{207}Pb/^{235}U$ diagram (Wetherill Concordia), allowing to calculate an upper intercept date of 3091 ± 13 Ma (MSWD = 4.2; n = 47; Fig. 6A; Table 3). This date is interpreted as the emplacement age of the dyke. Six other analyses give discordant results and were not included in calculation, and one grain is concordant and gives a concordia date of 3158 ± 28 Ma. This grain is interpreted as a xenocryst.

Sample PC04. This sample yielded only a few small zircon grains. The grains are euhedral, prismatic (1:2 to 1:1) and pinkish to reddish. In CL, the grains exhibit a well-defined oscillatory zoning (Fig. 5B) suggesting a magmatic origin, which is further corroborated by the Th/U ratios of the grains, ranging between 0.52 and 0.80 (Appendix 4).

Only five grains were suitable for analysis (seven analyses), among which three analyses are discordant and four analyses (3 grains) are concordant and allow to calculate a concordia date of 3087 ± 13 Ma (MSWD = 1.3, probability of concordance and equivalence = 0.25; Fig. 6B). Assuming the three grains used to calculate this date are autocrysts, the 3087 ± 13 Ma date is interpreted as the emplacement age of the dyke.

4.2. Geochronological results for the Igarapé Bahia Group

Cathodoluminescence images of representative grains and geochronological results are presented in Figs. 7 and 8, respectively. Analytical results are available in the Appendix 5 and geochronological diagrams for each sample including both concordant and discordant analyses in Appendix 6.

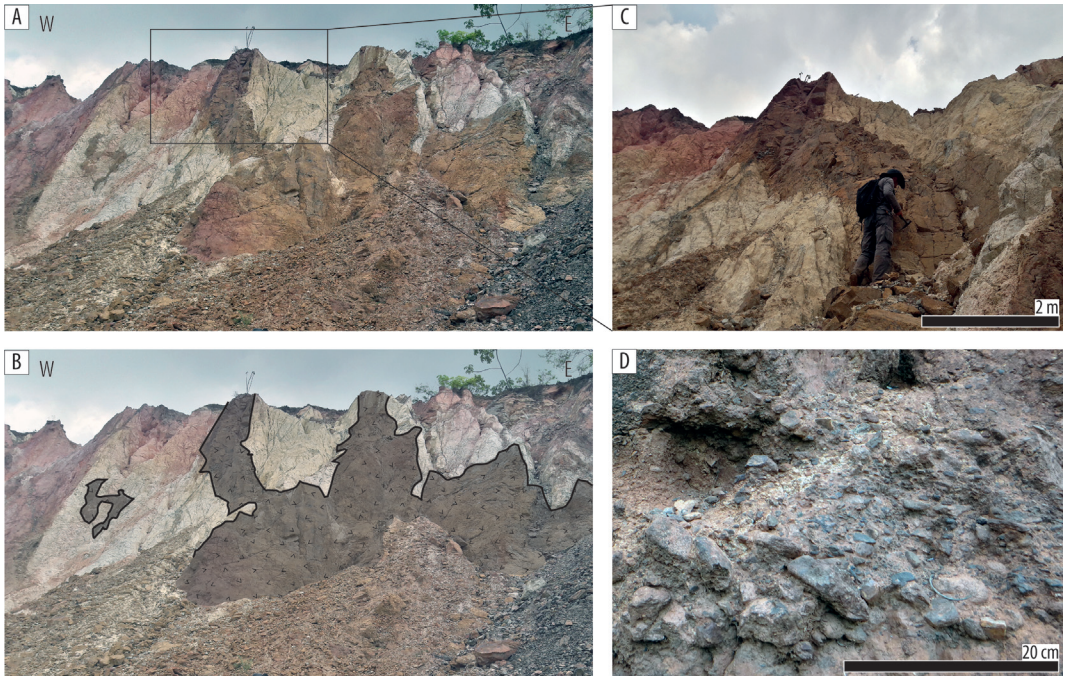

Fig. 4. Rio Novo Group – Field pictures. (A) Overview of a mafic dyke intruding the Rio Novo phyllites. Sample PC01 has been collected within this dyke. (B) Interpretation. Weathered phyllites and weathered mafic dyke. (C) Close up view. (D) Clasts supported conglomerate of the Rio Novo Group showing oblate, rounded and imbricated clasts.

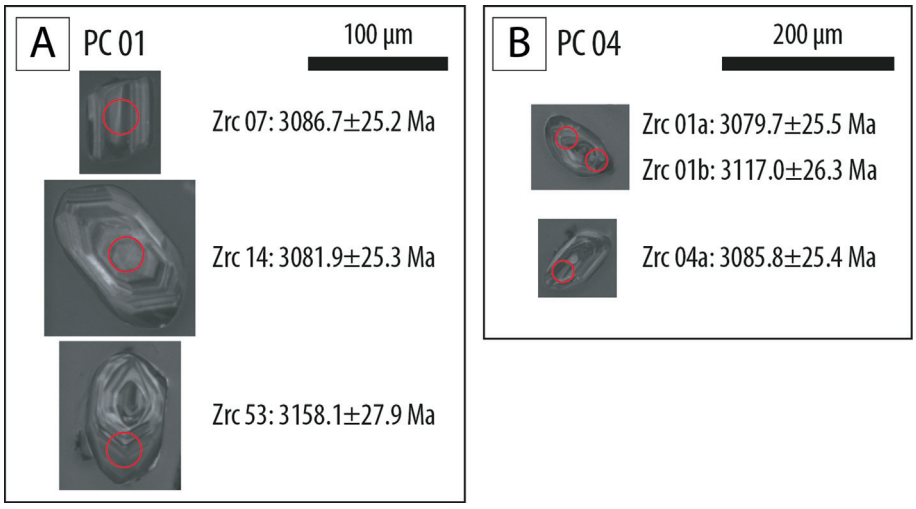

Fig. 5. Cathodoluminescence images of representative zircon grains of dolerite dykes intruding the Rio Novo Group. (A) Sample PC 01. (B) Sample PC 04. Red circles indicate the location of analyses. Uncertainties are given at the 2σ level.

Sample GT12 56.00–56.20. Most of the grains from this conglomerate are euhedral, slightly elongated, sometimes contain inclusions and exhibit a translucent to pinkish color. Other grains are rounded to angular with pinkish, reddish, yellowish or brownish colors. About 100 grains have been thermally annealed and chemically abraded (TACA treatment), after which most of the grains became translucent with a spotless texture. A few grains showed an orange or reddish to brownish color and a strongly etched texture. These etched grains are non-luminescent in CL and gave discordant dates indicating that the TACA treatment has not been efficient on these grains. In CL, the translucent and spotless grains exhibit a well-defined oscillatory zoning typical of magmatic zircon (Fig. 7A). Such a magmatic origin is also corroborated by Th/U ratios ranging from 0.43 and 1.42.

The youngest cluster, defined by 11 grains, gives a concordia date of 2762.6 ± 8.7 Ma (MSWD = 0.32, probability = 1.00; Table 2), interpreted as the MDA for this conglomerate (Fig. 8A). Other grains have Neo- to Mesoarchean ages, up to 2998 ± 28 Ma.

Sample FD02 118.80–119.15. This sandstone yielded a rather limited amount of zircon grains, exhibiting uniform shapes and colors. Most of the grains are angular or euhedral, sometimes contain inclusions, and display translucent to slightly pinkish colors. Other grains are angular to sub-rounded and display pinkish, yellowish or reddish colors. Only five grains were recovered after TACA treatment, after which the grains became translucent with a spotless texture. Both oscillatory zoning in CL (Fig. 7B) and Th/U ratios ranging from 0.39 and 0.71 support a magmatic origin for these grains.

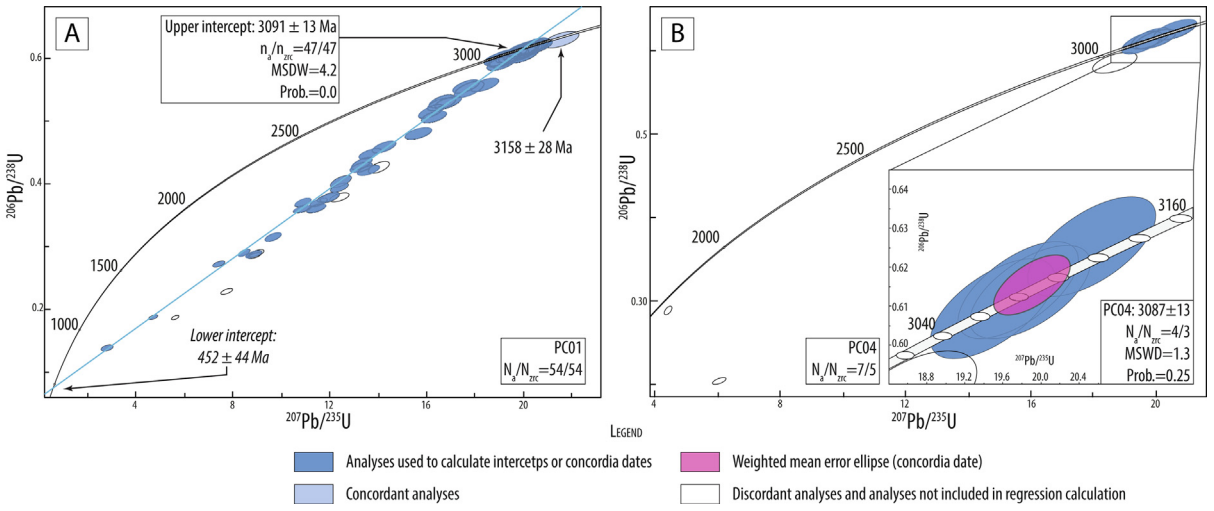

Fig. 6. Geochronological diagrams for dolerite dykes intruding the Rio Novo Group. (A) Sample PC 01. (B) Sample PC 04. All the diagrams were generated using Isoplot/Ex 3.00 (Ludwig, 2012). Error ellipses are depicted at the 2σ level. N_a: number of analyses; N_{zrc}: number of zircon grains; MSWD: Mean Square Weighted Deviate (given for both concordance and equivalence when referring to a concordia date); Prob.: probability if fit of the regression (upper intercept date) or probability for concordance and equivalence (concordia date).

Three out of the five concordant grains define a concordia date of 2705 ± 16 Ma, interpreted as the MDA for this sample (Fig. 8A). The two other concordant grains have older ages of 2842 ± 37 Ma and 3150 ± 31 Ma.

4.3. Geochronological results for the Rio Fresco Group

Sample DH01 103.64–103.75. This sandstone contains numerous zircons grains that are rather small and exhibit euhedral to sub-angular shapes. Euhedral grains are prismatic, with a length to width ratio comprised between 1:1 and 3:1. The grains display pinkish color and have apparent uniform characteristics in terms of color, grain-size and shape. In CL, most of the grains exhibit oscillatory zoning typical of magmatic zircon (Fig. 7A), but some grains show a faint zoning or are not zoned. The Th/U ratios of concordant grains range between 0.26 and 2.01, also consistent with a magmatic origin.

The youngest cluster, defined by 10 analyses on 10 grains, gives a concordia date of 2819 ± 11 Ma (MSWD = 0.92, probability = 0.55; Table 2), interpreted as the maximum depositional age for this sandstone (Fig. 8A). Other concordant dates spread from the maximum depositional age up to ca. 2860 Ma. Three grains plot around 2940 Ma, and three other grains have Meso- to Paleoarchean ages, at 3301 ± 31 Ma, 3339 ± 33 Ma and 3512 ± 30 Ma. In addition, three grains are younger than the preferred maximum depositional age. These grains do not define a single cluster and give dates of 2518 ± 31 Ma, 2624 ± 34 Ma and 2669 ± 24 Ma. These dates suggest that the deposition of the sediment could be younger, i.e., the deposition could have occurred during the Paleoproterozoic. However, these grains do not form a single cluster, and as no separate aliquot has been analyzed to test reproducibility, the statistical requirements are not met to confidently consider these younger dates as a maximum depositional age (Spencer et al., 2016).

Sample DH01 184.70–185.00. This sandstone, collected in the same drill core as sample DH01 103.64–103.75, also yielded numerous zircon grains exhibiting rather similar morphological characteristics, with most grains being small with euhedral to sub-angular shapes. A few grains are sub-rounded. Euhedral grains are prismatic to slightly elongated, with a length to width ratio comprised between 1:1 and 3:1. A few grains are more elongated, with a length to width ratio of 5:1 or more. The grains display pinkish to reddish color. Because only 7.3% of the analyzed grains in sample DH01 103.64–103.75 were concordant, zircon grains from sample DH01 184.70–185.00 have been thermally annealed and chemically abraded (TACA treatment) before LA-ICP-MS analyses to tackle this very low concordance rate issue. A large number of grains has been randomly picked up for TACA treatment, and most of the grains were recovered after this TACA treatment, among which ~ 350 grains were mounted. The majority of the grains became translucent and display a spotless to slightly etched surface, even though some grains remained slightly pinkish or exhibit a reddish to brownish color and a strongly etched surface after TACA treatment. In CL, most of the grains exhibit a well-defined oscillatory zoning and a have a very bright CL intensity (Fig. 7B), suggesting a magmatic origin. Some grains exhibit a more complex internal structure or display a core-rim structure (Fig. 7B), and most of the concordant grains have Th/U ratios higher than 0.1, compatible with a magmatic origin. Seventy-two out of 196 analyses obtained from TACA grains are concordant, giving a ratio of concordant analyses of 36.7%.

The youngest cluster, defined by three grains, gives a concordia date of 2723 ± 16 Ma (MSWD = 1.3, probability = 0.25; Table 2). This date is interpreted as the MDA for this sandstone. The other concordant grains spread from the MDA to the Eoarchean, at 3643 ± 28 Ma (Fig. 8A). A unique grain yielded a concordant date of 2668 ± 27 Ma that is younger than the preferred maximum depositional age. However, the statistical requirements are not met to confidently consider this date as an MDA, and we keep the conservative interpretation of 2723 ± 16 Ma as the maximum depositional age for this sandstone.

Sample DH02 173.85–173.95. This siltstone to fine sandstone yielded a lot of small grains. Most of the grains are euhedral with prismatic (length to width ratio of 1:1) to elongated (length to width ratio of 4:1) shapes. Some grains also display sub-angular and sub-rounded shapes. The grains exhibit various colors, from translucent to pale pink to reddish and brownish shades and are oscillatory zoned, which is typical of magmatic zircon (Fig. 7C). The Th/U ratios of concordant grains range between 0.56 and 2.28, also supporting a magmatic origin.

The youngest cluster gives a concordia date of 2908 ± 12 Ma (n = 8, MSWD = 0.94, probability = 0.52; Table 2). This date is interpreted as the MDA for this sample. The other concordant grains spread from the MDA to the Mesoarchean, at 3092 ± 35 Ma (Fig. 8A). A single grain yielded a concordant date of

Fig. 7. Cathodoluminescence images of representative zircon grains of the Azul Formation. Red circles indicate the location of analyses. Uncertainties are given at the 2σ level. (A, B) Igarapé Bahia Group. (C–I) Rio Fresco Group. (A) Sample GT12 56.00–56.20. (B) Sample FD02 118.80–119.15. (C) Sample DH01 103.64–103.75. (D) Sample DH01 184.70–185.00. (E) Sample DH02 173.85–173.95. (F) Sample DH02 175.80–175.90. (G) Sample DH02 175.80–175.90. (H) Sample DH03 63.05–63.25. (I) Sample DH03 198.05–198.30.

2661 ± 32 Ma, younger than the preferred maximum depositional age, but the statistical requirements are not met to confidently consider this date as an MDA.

Samples DH02 175.80–175.90 and DH02 177.94–178.00. These two sandstone samples, which are ca. 2 m apart in the DH02 drill core, are presented together because they have essentially similar characteristics regarding their zircon content. Both samples yielded a limited number of small zircon grains, translucent to pale pink in color, with euhedral and prismatic to elongated shapes (1:1 to 4:1). A few grains are sub-angular to rounded. In CL, the grains exhibit a well-defined to faint oscillatory zoning typical of magmatic zircon and some grains exhibit a core and rim internal structure (Fig. 7D, E). The Th/U ratios of concordant grains are higher than 0.1, also supporting a magmatic origin.

The youngest cluster in sample DH02 175.80–175.90 gives a concordia date of 2884 ± 17 Ma (n = 4, MSWD = 1.20, probability = 0.28; Table 2). This date is interpreted as the MDA for this fine sandstone. Another grain is older than the MDA, with a concordia date of 2994 ± 34 Ma (Fig. 8A). Here again, a single grain yielded a concordant date of 2816 ± 32 Ma, younger than the preferred MDA, but the statistical requirements are not met to confidently consider this date as an MDA. In sample DH02 177.94–178.00,

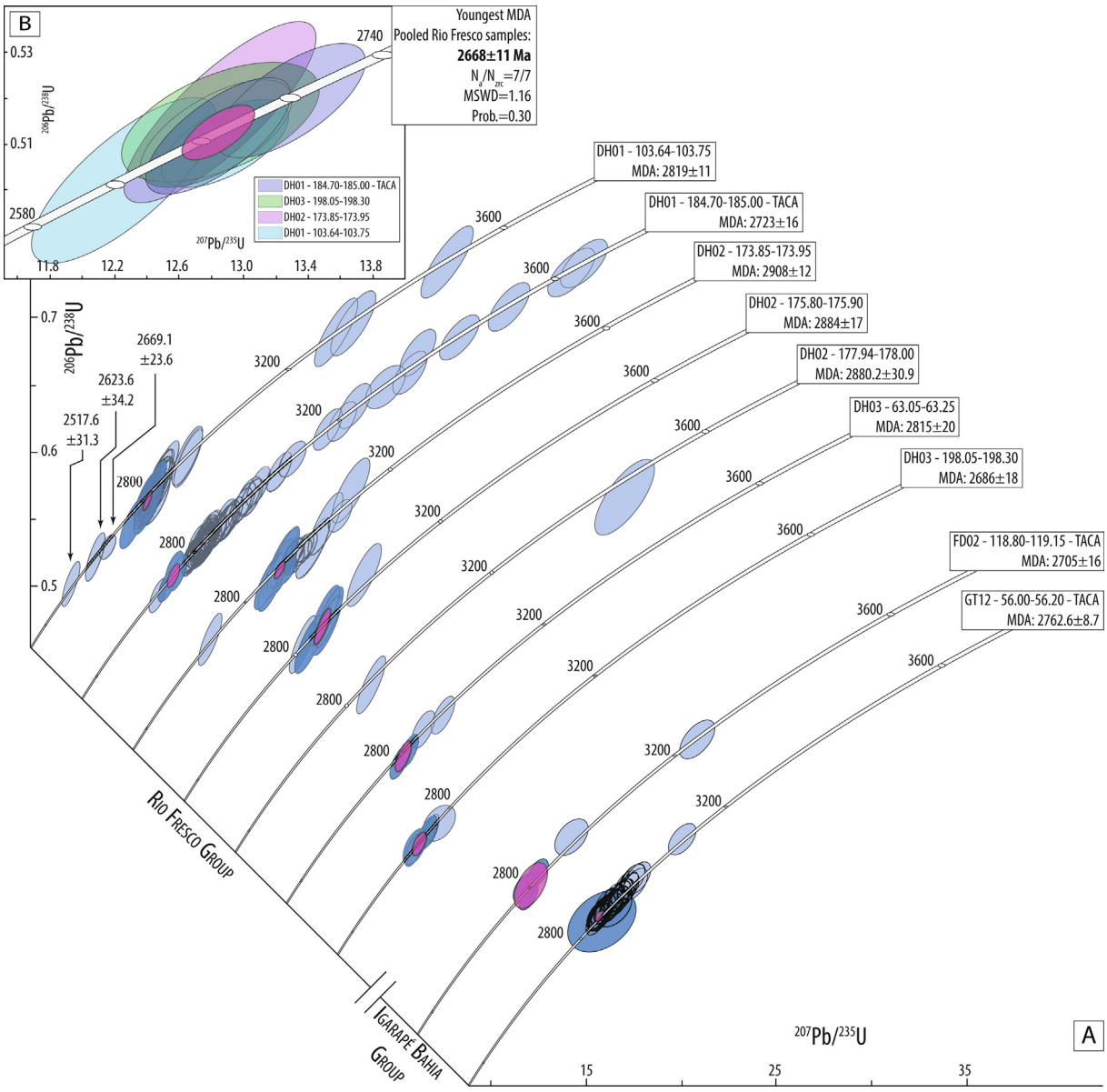

Fig. 8. Geochronological diagrams for the Azul Formation. (A) Analyses used to calculate the Maximum Depositional Age (MDA) are depicted in dark blue. Other concordant analyses are depicted by pale blue. The weighted mean error ellipse (concordia date) of the youngest cluster of concordant grains is depicted in pink. Samples collected in the same drill cores are presented according to their stratigraphic position (i.e., samples collected in the bottom of the drill cores to the bottom, samples collected to the top of the drill cores to the top). The number of analyses, the mean square weighted deviate for concordance and equivalence and the probability for concordance and equivalence for each MDA are provided in Table 2. (B) Maximum depositional age calculated from the youngest grains of five samples, assuming the grains are cogenetic in origin. N_a: number of analyses; N_{zrc}: number of zircon grains; MSWD: Mean Square Weighted Deviate for concordance and equivalence; Prob.: probability for concordance and equivalence. All the diagrams were generated using Isoplot/Ex 3.00 (Ludwig, 2012). Error ellipses are depicted at the 2σ level.

the two concordant grains give concordia dates of 2880 ± 32 Ma and 3475 ± 41 Ma.

Sample DH03 63.05–63.25. This fine sandstone yielded a limited number of zircon grains, which display rather diversified shapes, colors and grain sizes. Some grains are euhedral, prismatic (2:1 to 3:1) and display a pinkish color. Other euhedral grains, commonly very small, display a more elongated shape (5:1) and are translucent. The other grains, generally exhibiting a slightly coarser grain size, display various shapes (from angular to rounded) and various colors (pinkish, orange, brownish). In CL, the grains exhibit a well-defined to faint oscillatory zoning typical of magmatic zircon (Fig. 7F), also supported by Th/U ratios of concordant grains ranging between 0.45 and 1.21.

The youngest cluster, defined by only two grains, gives a concordia date of 2815 ± 20 Ma (MSWD = 1.20, probability = 0.31; Table 2). This date is provisionally interpreted as the MDA for this sandstone, but further analyses are required to meet statistical requirements and validate this date as a definite MDA. The two other concordant grains spread from the MDA to the Mesoarchean, at 2940 ± 28 Ma (Fig. 8A).

Sample DH03 198.05–198.30. This fine sandstone yielded a limited number of zircon grains displaying rather homogeneous shapes, colors and grain sizes. Most of the grains are small and exhibit euhedral (1:1 and 3:1) to sub-angular shapes, with a pinkish color. A few euhedral grains are elongated and translucent. Other grains display rounded to sub-rounded shapes and various pinkish, orange or brownish colors. In CL, the grains exhibit oscil-

latory zoning typical of magmatic zircon (Fig. 7G). The Th/U ratios of concordant grains range between 0.54 and 1.01, also consistent with a magmatic origin.

The youngest cluster gives a concordia date of 2686 ± 18 Ma (n = 3, MSWD = 1.7, probability = 0.14; Table 2). This date is interpreted as the MDA for this sample. Two other grains are slightly older, with concordia dates of 2732 ± 27 Ma and 2757 ± 41 Ma (Fig. 8A).

Summary. The MDA of sample DH03 198.05–198.30 (2686 ± 18 Ma) is the youngest one obtained in the Azul Formation. Assuming the youngest grains present in different samples of the Azul Formation derive from a single cogenetic source as suggested by their homogeneous Th/U ratio (0.80 ± 0.21), this gives a slightly more precise date of 2668 ± 11 Ma (n = 7, MSWD = 1.16, probability = 0.30; Table 2, Fig. 8B). This date, which is equivalent but slightly more precise than the MDA obtained for sample DH03 198.05–198.30 (Fig. 8A), is interpreted as the MDA for the Azul Formation.

4.4. Statistical analyses of zircon age distributions

The statistical analyses are performed through mixture modelling by an RJ-MC-MC approach to fit the age distribution of concordant grains obtained in the main sedimentary units of the Carajás Basin (Carajás Formation, Igarapé Bahia and the Rio Fresco groups). Mixture model results are provided in Table 4 and Fig. 9.

4.4.1. Carajás Formation

Description. The mixture model indicates that detrital zircon grains in the Carajás Formation belong to two main populations, among which one accounts for nearly all grains (96% of the total) and a second population comprises the remaining 4% of the grains. The main population (component 1; Table 4) has a mean age of ca. 2730 Ma, which is equivalent to the depositional age of the Carajás Formation, and a small standard deviation of 1 Myr (Table 4, Fig. 9A). The oldest population (component 2; Table 4) has a mean age of 2880 Ma and a large standard deviation of 112 Myr.

Interpretation. Mixture model results suggest that nearly all the detrital zircon grains from the Carajás Formation derive from a single and short-lived magmatic event that occurred during or slightly before the deposition of this formation. This detrital zircon population, collected in volcaniclastic samples, was probably formed during a volcanic pulse related to the emplacement of ultramafic and mafic rocks as well as A-type granitoids mainly between ca. 2760 Ma to ca. 2730 Ma (Barros et al., 2009; Feio et al., 2012, 2013; Machado et al., 1991; Melo et al., 2017; Sardinha et al., 2006). The oldest population found in the Carajás Formation may have originated from ca. 2870 Ma to 2830 Ma TTG rocks constituting part of the basement of the Carajás Domain (Feio et al., 2013; Machado et al., 1991; Moreto et al., 2015; Pidgeon et al., 2000).

4.4.2. Igarapé Bahia Group

Description. Five components were inferred by mixture modelling. As for the Carajás Formation, the youngest population, with a mean age of 2722 Ma, has rather small standard deviation of 17 Myr, but this population represents only 18% of the detrital zircon grains, compared to 96% in the Carajás Formation (Table 4, Fig. 9B). The four older populations correspond to longer magmatic or metamorphic events (standard deviations comprised between 35 Ma and 80 Ma; Table 4) that occurred around 2804 Ma, 2937 Ma, 3014 Ma and 3101 Ma (Fig. 9B). These populations have variable relative contributions, ranging from 7% for the component 5 to 31% for the component 3 (Table 4).

Interpretation. The youngest zircon population was probably sourced from the erosion of magmatic rocks related to the ca. 2760 Ma to ca. 2730 Ma magmatic event represented by ultramafic and mafic rocks as well as A-type granitoids (Machado et al., 1991; Sardinha et al., 2006; Barros et al., 2009; Feio et al., 2012, 2013; Melo et al., 2017). The origin of the detrital population with a mean age of 2804 Ma is more elusive, because this population seems to be younger than the ca. 2870 Ma to 2830 Ma TTGs occurring in the basement of the Carajás Domain (Feio et al., 2013; Machado et al., 1991; Moreto et al., 2015; Pidgeon et al., 2000). However, the Rio Verde trondhjemite, which is probably related to the ca. 2870 Ma to 2830 Ma magmatic episode, has an age of 2820 ± 22 Ma (Feio et al., 2012) and represents a likely source for the 2804 Ma detrital population. The 2937 Ma population matches well the age of the ca. 2960 Ma to ca. 2930 Ma TTG from the basement of the Carajás Domain (Feio et al., 2013) and could have been sourced by the erosion of these TTGs. The 3014 Ma population fits the age of the oldest basement rocks of the Carajás Domain, which were emplaced between ca. 3080 Ma and ca. 3000 Ma (Machado et al., 1991; Pidgeon et al., 2000; Moreto et al., 2015). The oldest population, with a mean age of 3101 Ma, likely corresponds to the magmatic event responsible for the emplacement of mafic dykes intruding the Rio Novo Group (this study).

Table 4
Mixture modeling results.

Carajás Formation Model results for 2 components	Mean age (Ma)	Standard deviation (Myr)	Contribution (%)
Component 1	2730 (2729–2730)	1 (0–5)	96 (94–98)
Component 2	2880 (2803–2956)	112 (57–150)	4 (2–6)
Igarapé Bahia Group			
Model results for 5 components	Mean age (Ma)	Standard deviation (Myr)	Contribution (%)
Component 1	2722 (2713–2733)	17 (2–28)	18 (8–26)
Component 2	2804 (2770–2818)	35 (16–60)	29 (10–45)
Component 3	2937 (2809–2977)	71 (24–149)	31 (3–50)
Component 4	3014 (2941–3068)	72 (7–150)	16 (2–49)
Component 5	3101 (2986–3293)	80 (6–150)	7 (0–35)
Rio Fresco Group			
Model results for 5 components	Mean age (Ma)	Standard deviation (Myr)	Contribution (%)
Component 1	2672 (2592–2688)	13 (1–105)	9 (1–15)
Component 2	2816 (2676–2839)	24 (0–145)	22 (2–34)
Component 3	2873 (2830–2920)	93 (79–150)	33 (5–63)
Component 4	2964 (2887–3357)	95 (25–150)	29 (1–61)
Component 5	3399 (3294–3545)	145 (100–150)	7 (2–11)

Numbers in brackets refer to the credible intervals (95% confidence level) on each parameter of the modeled components (mean, standard deviation, contribution).

Table 5
Updated age constraints for the main sedimentary units of the Carajás Basin.

Number in Fig. 10	Method	Object	Interpretation	Age (Ma)	Reference
Rio Novo Group					
1	Zircon U-Pb	Mafic dyke intruding the Rio Novo Group	Minimum depositional age	3091 ± 13	This work
Parauapebas Formation					
2	Zircon U-Pb	Metabasalt	Depositional age	2750 ± 7	Martins et al., 2017
Carajás Formation					
3	Zircon U-Pb	Volcaniclastic layer	Depositional age	2720 ± 6	Rossignol et al., submitted
Igarapé Bahia Group					
4	Zircon U-Pb	Sandstones to conglomerates	Maximum depositional age	2684 ± 10	Rossignol et al., 2020a
5	Monazite U-Pb	Hydrothermal vein	Minimum depositional age	2575 ± 12	Tallarico et al., 2005
Azul Formation					
6	Zircon U-Pb	Sandstones	Maximum depositional age	2668 ± 11	This work
7	Zircon U-Pb	Sandstones	Youngest detrital zircon grain from the Azul Formation, should be considered cautiously as it is defined by only one grain	2518 ± 31	This work
8	Zircon U-Pb	Granite intruding the Águas Claras Formation	Minimum depositional age	1880 ± 2	Machado et al., 1991

Uncertainties are given at the 2σ level.

4.4.3. Rio Fresco Group

Description. This sedimentary unit comprises five main populations. The youngest one represents 9% of the zircon grains, with a mean age of 2672 Ma and a rather small standard deviation of 13 Myr (Table 4, Fig. 9C). About 22% of the zircon grains from the Rio Fresco Group belong to an older population characterized by a mean age of 2816 Ma and a standard deviation of 24 Myr. The two largest populations of the Rio Fresco Group have contributions of 33% and 29%, mean ages of 2873 Ma and 2964 Ma and standard deviations of 93 Myr and 95 Myr, respectively (Table 4, Fig. 9C). The oldest modelled population is Paleoarchean in age (3399 Ma) and contributes 7% of the zircon grains.

Interpretation. Because mixture modelling infers a rather large number of populations (k = 5) based on a rather low number of grains (n = 202), these results should be considered with caution, especially regarding the relative contribution of each population (Licht et al., 2016). However, the mean ages of some populations clearly show that the components found in the Rio Fresco differ from those found in the underlying Igarapé Bahia Group. The age of the youngest population compares well with those of ca. 2670 Ma tonalites exposed in the Bacajá Domain (Macambira et al., 2009), suggesting that ~ 9% of the grains were sourced from a remote northern location (present day coordinates). Three other populations, with mean ages of 2816 Ma, 2873 Ma and 2964 Ma likely derive from TTG forming the basement of the Carajás Domain (Feio et al., 2012, 2013; Machado et al., 1991; Moreto et al., 2015; Pidgeon et al., 2000). TTG and sanukitoid suites from the Rio Maria Domain, which were emplaced between ca. 2960 Ma and ca. 2920 Ma (Almeida et al., 2013), and between ca. 2870 Ma and ca. 2860 Ma (Almeida et al., 2013; Althoff et al., 2014; Feio et al., 2013; Macambira and Lancelot, 1996), could also have contributed to the 2873 Ma and 2964 Ma populations found in the Rio Fresco Group. No Paleoarchean rocks with an age matching the 3399 Ma population of the Rio Fresco Group have been recorded, neither in the Carajás nor in other domains of the Amazonia Craton. However, this age fits well with Hf crustal model ages calculated from zircon grains collected in the Parauapebas Formation (Martins et al., 2017), suggesting that the basement of the Carajás Domain preserves Paleoarchean relics.

5. Discussion

5.1. Paleoarchean to early Mesoarchean sedimentary record

The zircon grains collected in two mafic dykes intruding the Rio Novo Group show textural and chemical features typical of a magmatic origin, pointing toward autocrystic minerals. The dykes were emplaced at ca. 3.1 Ga (Fig. 6) and are probably related to the ca. 3080–3000 Ma magmatic event documented in the Carajás Domain (Machado et al., 1991; Pidgeon et al., 2000; Moreto et al., 2015).

The emplacement age of the dykes implies that the Rio Novo Group is older than ca. 3.1 Ga (Fig. 10A). Although the exact age of the Rio Novo Group remains unknown, it represents one of the oldest sedimentary unit known in South America. Such finding suggests that the Carajás Domain was already rigid enough to sustain the accumulation and preservation of sedimentary basins by the early Mesoarchean or before. This is in line with the occurrence of a ca. 3.2 Ga to ca. 3.4 Ga Paleoarchean basement in the Carajás Domain hypothesized from Hf crustal model ages of zircon grains from the Parauapebas Formation (Martins et al., 2017). Together with the occurrence of Paleo- and Eoarchean zircon grains in the Rio Fresco Group (this work) and evidence supporting the presence of an Eoarchean recycled crust in the Guyana Shield (Milhomem Neto and Lafon, 2019), these findings suggest that ancient Eoarchean to Paleoarchean nuclei form the backbone of the Amazonia Craton. These nuclei probably amalgamated together during the course of the Mesoarchean, and the collision between such small continental blocks could be related to the end-Mesoarchean stratigraphic hiatus that spanned at least 300 Myr in the Carajás Basin (Fig. 10A, B).

5.2. The Parauapebas large Igneous Province and associated iron formations

During the beginning of the Neoarchean, the Carajás Domain experienced a major magmatic event represented by the volcanic rocks of the Parauapebas Formation and by various intrusive magmatic rocks including layered ultramafic and mafic plutons, as well as A-type granitoids mainly emplaced between ca. 2760 Ma to ca. 2730 Ma (Barros et al., 2009; Feio et al., 2012, 2013; Machado et al.,

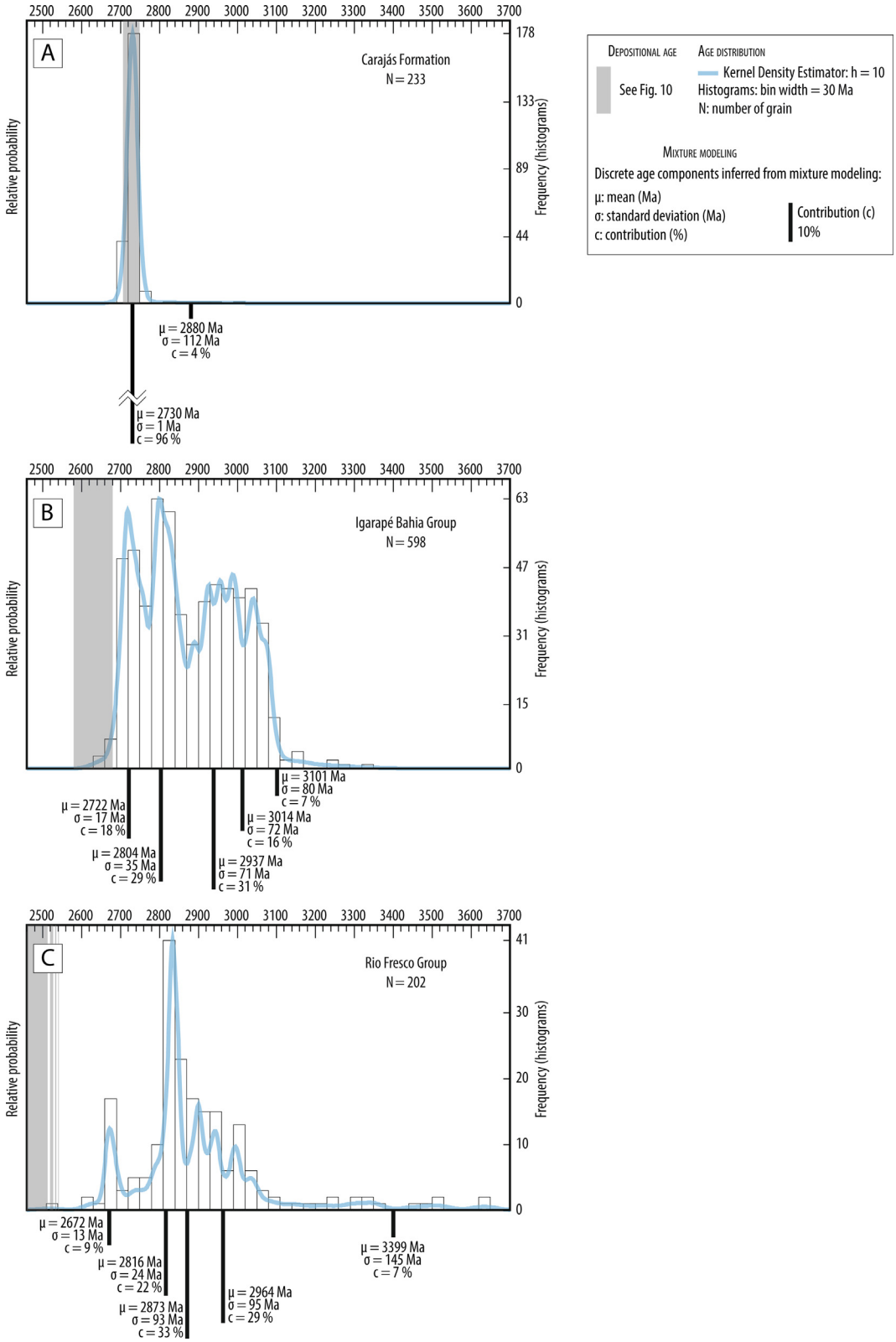

Fig. 9. Age distribution and main detrital age components. The discrete age components, their relative contributions and width in age distributions were determined by a RJ-MC-MC performed with Bayes Mix (after Jasra et al., 2006; Gallagher et al., 2009). Confidence levels on each parameter are presented in the Table 4. Parameters values and acceptance rates are available in the Appendix 3. The age distributions and histograms were generated with Density Plotter 8.5 (after Vermeesch, 2012).

1991; Mansur and Ferreira Filho, 2016; Sardinha et al., 2006; Siepierski and Ferreira Filho, 2020). The occurrence of several layered ultramafic intrusions has led a Neoarchean Large Igneous Province (LIP) being inferred in the Carajás Domain (Siepierski and Ferreira Filho, 2020; Fig. 11). In the following, we review the characteristics of this magmatic event in order to assess whether or not

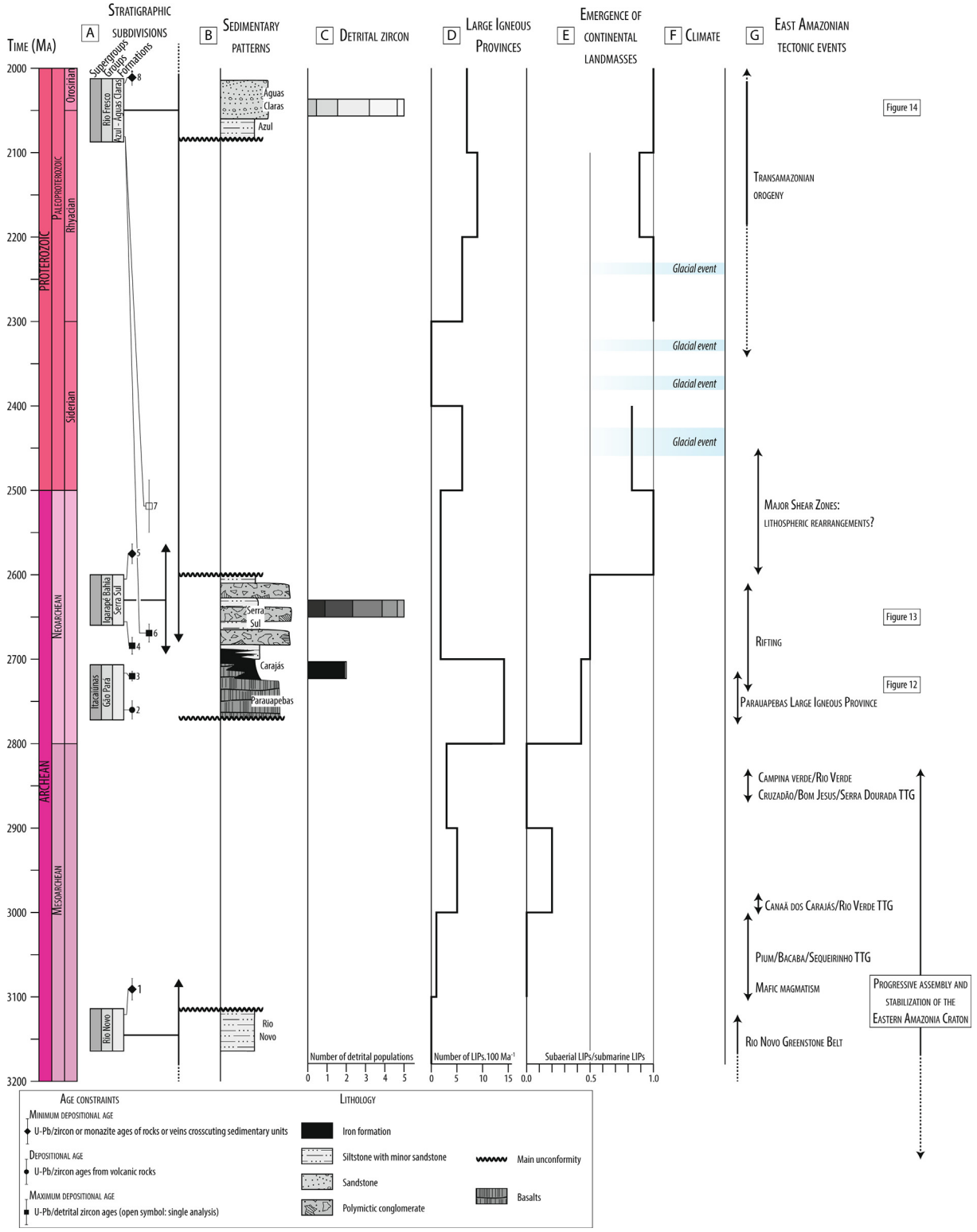

Fig. 10. Chart summarizing the main geodynamic events in the eastern Amazonia Craton and their relationship with global events. (A) Stratigraphic subdivisions for the main sedimentary units of the Carajás Basin. Numbers for age constraints refers to the Table 5. Arrows indicate range of potential ages for sedimentary units and unconformity separating them. Stratigraphic chart: International Chronostratigraphic Chart v2020/01 (after Cohen et al., 2013). (B) Sedimentary patterns. (C) Histogram showing the number of detrital zircon populations inferred from mixture modelling. For each sedimentary unit, sizes of individual boxes are proportional to the relative contribution of each populations. (D) Histogram showing the number of LIPs for 100 million years age range, from the database of Kump and Barley (2007). (E) Emergence of continental landmasses using the proportion of subaerial LIPs as a proxy for emerged landmasses. Proportion determined as the percentage of the total subaerial LIP occurrences in the age range divided by the total occurrence of both subaerial and submarine LIPs in that age range, using the methodology and database of Kump and Barley (2007). (F) Glacial events. Ages after Rasmussen et al. (2013) and Gumsley et al. (2017). (G) Synthesis of the main tectonic events that occurred in eastern Amazonia Craton. TTG: Tonalites, Trondhjemites and Granodiorites.

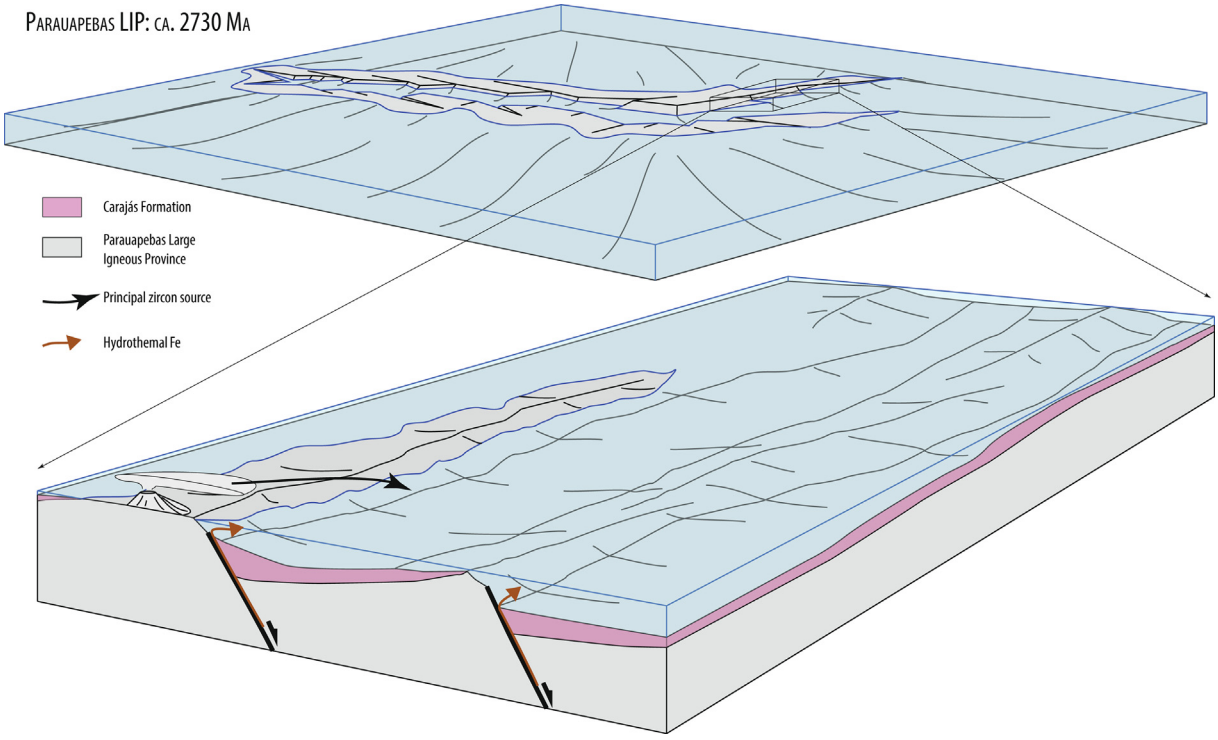

Fig. 11. Reconstruction of the Parauapebas LIP and associated sedimentary system.

Table 6
Main features of the Parauapebas magmatic event and comparison with LIPs' characteristics.

LIP characteristics	Parauapebas volcanics and associated intrusive rocks	Additional remarks
Spatial extent > 10^5 km^2	Distribution of inliers of Parauapebas volcanics over a > 370 km long strike (Souza et al., 2020; Vasquez et al., 2008). Assuming a radial distribution encompassing all outliers, the area covered by the basalts of the Parauapebas Formation is above 10^5 km^2.	Minimum areal extent, because Parauapebas volcanics are covered to the west by the Uatumã SLIP and truncated to the East by the Araguaia Belt
Volume of magmatic rocks > 10^5 km^3	Thickness of the Parauapebas Formation comprised between 4 and 6 km (Olszewski et al., 1989; Lacasse et al., 2020). Assuming a radial distribution and a thickness of 4 km gives a volume much higher than 10^5 km^3	The thickness of Parauapebas is poorly constrained. The value estimated here is likely a minimum estimate, because the volume of intrusive rocks is not taken into account and the spatial extent of basaltic rocks is likely larger than the one considered here.
Duration of magmatism < 50 Ma	Most of the Parauapebas volcanics were outpoured during a ~ 20 Myr interval, from ca. 2770 Ma to ca. 2750 Ma (Wirth et al., 1986; Olszewski et al., 1989; Machado et al., 1991; Trendall et al., 1998; Martins et al., 2017). Associated intrusive rocks were emplaced from ca. 2760 Ma to ca. 2730 Ma (Barros et al., 2009; Feio et al., 2012, 2013; Machado et al., 1991; Sardinha et al., 2006).	
Pulsed nature of magmatism	Mixture model result indicates that zircon grains deriving from the Parauapebas volcanics were produced during a short-lived magmatic event (~1 Myr).	Crystallization age of zircon grains provides only a partial figure of the dynamic of the Parauapebas magmatism.
Tectonic setting	Continental rift (Olszewski et al., 1989; Feio et al., 2012; Martins et al., 2017; Tavares et al., 2018; Toledo et al., 2019; Lacasse et al., 2020).	A back-arc basin setting (Dardenne et al., 1988) is ruled out by detailed analyses of geochemical alteration (Lacasse et al., 2020).
Composition	Mafic-dominant composition (Lacasse et al., 2020).	Basalts were produced by the partial melting of a depleted mantle source that assimilated country rocks and underwent fractional crystallization (Lacasse et al., 2020), supporting an intraplate setting.
Layered intrusions	Occurrence of nine well-exposed layered intrusions made up of dunnites, lherzolites, harzburgites, anorthosite and gabbros (Machado et al., 1991; Siepierski and Ferreira Filho, 2020).	Layered intrusions likely form the plumbing system of the Parauapebas LIP.
Silicic magmatism	A-type granitoids emplaced from ca. 2760 Ma to ca. 2730 Ma (Machado et al., 1991; Sardinha et al., 2006; Barros et al., 2009; Feio et al., 2012, 2013).	A-type granitoids rocks represent HT melting of the lower crust. A few HT-LP leucogranites (Sardinha et al., 2006) might correspond to the partial fusion of the upper crust.
Dyke swarms and sills	Not recognized.	Their presence is possible but likely covered by dense vegetation and/or extremely weathered.
Undersaturated magmatism (carbonatites, kimberlite)	Not recognized.	

LIP characteristics after Bryan and Ernst (2008).

it can be classified as a LIP according to the definition of Bryan and Ernst (2008), that is a "magmatic province with areal extent > 10^5 km^2, igneous volume > 10^5 km^3 and maximum lifespans of ~50 Myr that have intraplate tectonic settings or geochemical affinities, and is characterized by igneous pulse(s) of short duration (~1–5 Myr), during which a large proportion (>75%) of the total igneous volume has been emplaced" (Table 6). The Parauapebas Formation covers most of the present day Carajás Domain and inliers of basaltic rocks are distributed over > 370 km long strike (Souza et al., 2020; Vasquez et al., 2008). Assuming a radial distribution of basaltic rocks, the Parauapebas Formation would have covered an area larger than 10^5 km^2, consistent with that of a LIP (Bryan and Ernst, 2008; Table 6). In addition, the actual extent of Parauapebas Formation is likely larger because the Carajás Basin continues beneath the Uatumã Supergroup to the west (Fig. 3). The volume of the Parauapebas basalts is large enough to correspond to a LIP (Bryan and Ernst, 2008; Table 6). The overall duration of magmatism of the Parauapebas magmatic event lasted<50 Myr and is also consistent with a LIP (Bryan and Ernst, 2008). Volcanic eruptions occurred during a rather short time span, between ca. 2770 Ma and ca. 2750 Ma (Wirth et al., 1986; Olszewski et al., 1989; Machado et al., 1991; Trendall et al., 1998; Martins et al., 2017; Toledo et al., 2019), further supporting a LIP origin for the Parauapebas basalts. Intrusive rocks were emplaced during a slightly longer time interval, between ca. 2760 Ma to ca. 2730 Ma (Barros et al., 2009; Feio et al., 2012, 2013; Machado et al., 1991; Sardinha et al., 2006). The mixture model obtained with zircon grains from volcaniclastic rocks interbedded in the Carajás Formation suggests that the zircon population was produced during a short-lived magmatic event (as short as ~ 1 Myr; Table 4, Fig. 9A and 12). Various volcanic rocks, ranging from basalts to rhyolites, yielded similar emplacement ages (Wirth et al., 1986; Olszewski et al., 1989; Machado et al., 1991; Trendall et al., 1998; Martins et al., 2017), thus allowing to take the crystallization age of zircon grains as a rough estimate for the emplacement of volcanic rocks, from which the mixture model provides evidence for a transient nature of volcanism. Most of the igneous systems are characterized by pulses of magmatic output of various durations (de Saint Blanquat et al., 2011), and output of large volume of magma over a period of ~ 1 Myr is characteristic of LIP emplacement (Bryan and Ernst, 2008). Additional attributes suggest that the Parauapebas magmatic event might be classified as a LIP (Table 6). These include (i) a mafic-dominant composition of magmatic rocks (Lacasse et al., 2020), (ii) an intraplate tectonic setting (Olszewski et al., 1989; Feio et al., 2012; Martins et al., 2017; Toledo et al., 2019; Lacasse et al., 2020), (iii) the occurrence of several layered mafic–ultramafic intrusions (Machado et al., 1991; Siepierski and Ferreira Filho, 2020), and (iv) A-type granitoids that might correspond to subordinate high temperature silicic magmatic rocks documented in most LIPs (Bryan and Ernst, 2008).

The overall characteristics of the Parauapebas magmatic event thus suggest that it corresponds to a typical LIP (Bryan and Ernst, 2008), hereafter referred to as the Parauapebas LIP (Table 6, Fig. 11). The emplacement of LIPs has long been recognized to be associated with the deposition of BIFs, due to the contribution of magmatic activity and hydrothermal circulation as major Fe sources (Barley et al., 1997; Isley and Abbott, 1999; Abbott and Isley, 2002). The main zircon population in the Carajás Formation crystalized at the same time or slightly before the deposition of the Carajás BIFs (Fig. 9A and 12), indicating that the magmatic activity was still active at the time of deposition of BIFs and likely promoted hydrothermal circulation. The link between the Parauapebas LIP and Carajás BIFs is further corroborated by the source of Fe that derived from Fe-rich hydrothermal fluids (Lindenmayer et al., 2001; Klein and Ladeira, 2002; Macambira and Schrank, 2002; Rego et al., 2021). Because BIFs deposited in the Carajás Basin represent one of the world's largest iron deposits (Klein and Ladeira, 2002; Trendall, 2002; Dalstra and Guedes, 2004; Bekker et al., 2010; Hagemann et al., 2016), a substantial source of iron and important hydrothermal activity was necessary for their formation (Fig. 11).

5.3. Neoarchean rifting event

The formation of LIPs is commonly associated with continental rifting (Cox, 1989; Hill, 1991; Campbell, 2005), and the extension of the crust was initiated coeval with the emplacement of the Parauapebas basalts and the deposition of the Carajás BIFs, as shown by the large thicknesses' variations of BIFs, ranging from 100 m to 400 m throughout the basin (Beisiegel et al., 1973).

Detrital zircon provenance analysis of the Igarapé Bahia Group indicates that all populations can have been sourced by rocks forming the basement of the Carajás Basin, although the erosion of rocks of similar age from elsewhere in the Amazonia Craton could also have contributed to these populations. The fact that all detrital zircon populations can have been sourced by nearby areas is in line with the architecture of drainage networks in rift basins, which usually comprises numerous small transverse drainage divides (Gawthorpe and Leeder, 2000; Fig. 13). However, the cumulative zircon age distribution for the Igarapé Bahia Group points to a collisional setting (Fig. 12). Different explanations can account for such a discrepancy: (i) a tectonic style dominated by vertical motions (domes and keels), differing from the modern-style horizontal tectonics, could have prevailed during the deposition of the Igarapé Bahia Group (Bédard, 2018), although various lines of evidence point toward the onset of modern-style plate tectonic about 3.7 Ga or earlier, well before the deposition of the Igarapé Bahia Group (Turner et al., 2014; Bauer et al., 2020; Windley et al., 2021); (ii) the composition of sedimentary rocks, which represent potential source rocks for zircon grains, changed markedly throughout geological times, and volcaniclastic rocks presumably representing zircon fertile source rocks were much more common during the Archean that during the Phanerozoic (Ronov, 1972; Eriksson et al., 2005; Ernst, 2009). This might represent an important bias to the tectonic discrimination diagram of Cawood et al. (2012), because the latter has been established using a database comprising mainly Phanerozoic samples; (iii) in the specific case of the Igarapé Bahia Group the rather important contribution of zircon grains originating from the Parauapebas LIP (Table 4, Fig. 9B) could also have biased the tectonic setting inferred from the diagram of Cawood et al. (2012) by shifting the cumulative zircon age distribution toward the "convergent setting". The overall sedimentary pattern of the Igarapé Bahia Group (Fig. 10B), with thick and repetitive coarse-grained sediments deposited by downslope debris flows, as well as numerous sedimentary features attesting to high sedimentation rates and slope instability (Rossignol et al., 2020a) are consistent with those usually encountered in active extensional settings (Gawthorpe and Leeder, 2000). In addition, the co-occurrence of sedimentary facies indicative of shallow and deep-water environments suggests important relative sea-level variations during the deposition of the Igarapé Bahia Group, in line with subsidence mainly controlled by the rift tectonism (Dreher et al., 2005; Ribeiro da Luz and Crowley, 2012).

Despite that the depositional environments of the Grão Pará and the Igarapé Bahia groups remained essentially similar throughout the end of the Neoarchean, the nature of their sediments showed a dramatic change, from chemical iron formations to terrigenous deposits (Fig. 10B). This transition, although being well-marked, was progressive, as shown by the presence of a few BIF layers interbedded within terrigenous sediments toward the base of the Igarapé Bahia Group (Melo et al., 2019). This change

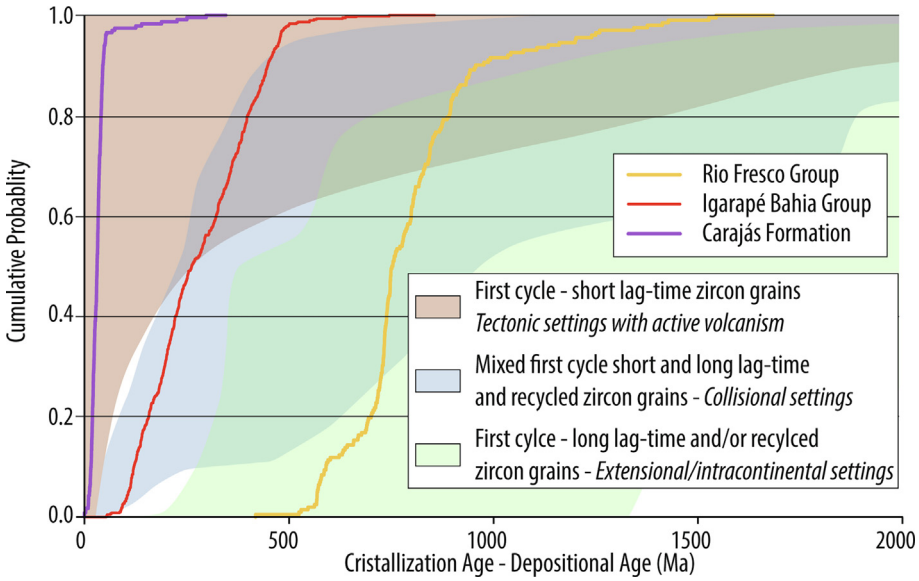

Fig. 12. Cumulative probability density plots and tectonic discrimination diagram based on the cumulative distribution of detrital grain ages. Depositional ages considered: Carajás Formation: 2710 Ma; Igarapé Bahia Group: 2600 Ma; Rio Fresco Group: 2100 Ma.

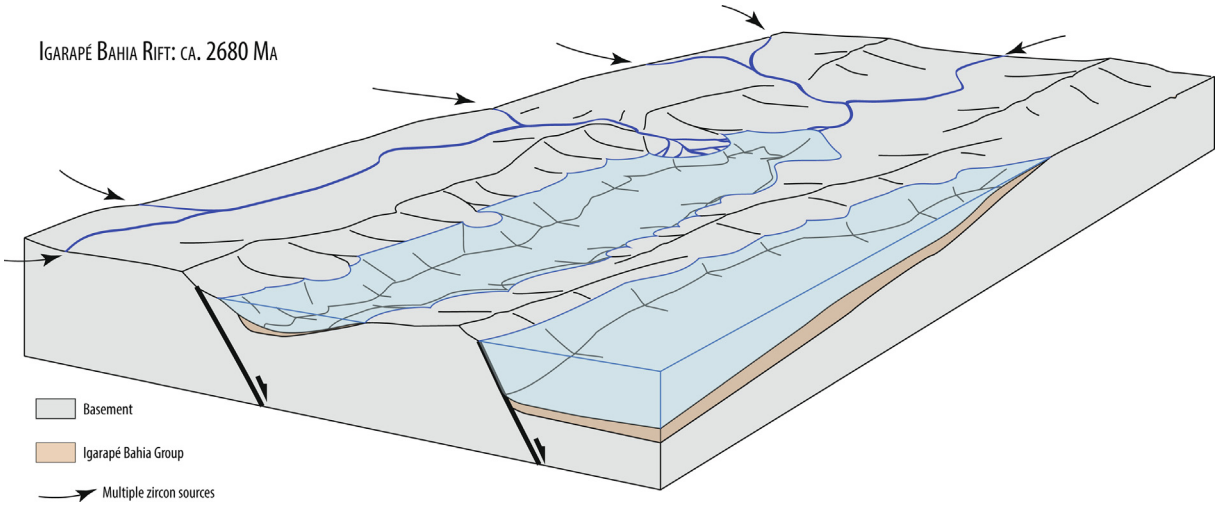

Fig. 13. Reconstruction of the Carajás Basin during the deposition of the Igarapé Bahia Group.

of sedimentary regime was likely accompanied by a decrease of Fe-rich hydrothermal fluid influx and an increase of terrigenous input into the basin. The decrease of Fe input can be related to the wanning activity of the Parauapebas LIP, but also to the worldwide decrease of LIP emplacement toward the end of the Neoarchean (Fig. 10D). The concomitant increase of terrigenous input into the basin could have been related to the uplift and emergence above sea level of the Amazonia Craton, resulting in an enhanced inland erosion that brought terrigenous material to the basin (Schröder et al., 2011). Such lowering of the sea level could have been related either to the regional tectonic activity, because the Carajás Basin corresponded to an active rift (Olszewski et al., 1989; Feio et al., 2012; Martins et al., 2017; Tavares et al., 2018; Toledo et al., 2019), or to eustatic variations linked to the global emergence of extensive landmasses above sea level by the end of the Neoarchean (Fig. 10E; Vlaar, 2000; Flament et al., 2008; Rey and Coltice, 2008; Pons et al., 2013; Bindeman et al., 2018). At that time, the strengthening of the continental lithosphere allowed for the development of emerged areas with significant topography (Flament et al., 2008; Rey and Coltice, 2008). This could have allowed for emersion and subsequent erosion of the hinterland of the Amazonia Craton, bringing terrigenous material to the Carajás Basin. On a global scale, the age of the rifting event in the southeastern Amazonia Craton broadly coincides in time with the break-up of one of the first documented supercontinents (Pehrsson et al., 2013; Gumsley et al., 2017; Salminen et al., 2019). Although speculative, because the location of the Amazonia Craton during the Neoarchean and the Paleoproterozoic remains unconstrained (Salminen et al., 2019), this hypothesis is in line with a similar tectonic evolution shared by the Limpopo Belt of the Kaapvaal Craton and the Carajás Domain (Feio et al., 2013), suggesting a connection between the Amazonia and Kaapvaal cratons. Based on these geological considerations, we propose that the Amazonia Craton could have been part of a large continental landmass, such as the proposed Supervaalbara supercontinent, along with the São Francisco, Superior, Wyoming, Kola and Karelia, Zimbabwe, Singhbhum, Tanzania, Yilgarn, and Pilbara cratons (Kumar et al., 2017; Salminen et al., 2019).

5.4. Paleoproterozoic evolution of the Carajás Basin

During the end of the Neoarchean and the beginning of the Paleoproterozoic, the Igarapé Bahia Group and older sedimentary units of the Carajás Basin have been affected by a long lasting tectono-thermal event between ca. 2600 Ma and 2450 Ma (Machado et al., 1991; Requia et al., 2003; Tallarico et al., 2005; Grainger et al., 2008; Melo et al., 2017; Toledo et al., 2019). The nature of this tectonic event remains elusive, as a very limited number of zircon grains produced during this episode were actually recovered in the Rio Fresco Group (e.g., one grain with a 2518 ± 31 Ma date might have been produced during this tectono-thermal event). This long-lasting tectonothermal event could be related to regional scale shear zones that reactivated older structures within the Carajás Domain (Melo et al., 2017, 2019; Toledo et al., 2019). This event marks the beginning of a long stratigraphic hiatus spanning several hundreds of millions of years (Fig. 10A) and compares with the widespread erosion of continental platforms reported in many places during the early Paleoproterozoic (Barley et al., 2005; Eriksson and Condie, 2014). Huronian glaciations occurred during this time period (Fig. 10F; Tang and Chen, 2013; Young, 2013) and are thus likely recorded as a stratigraphic surface in the Carajás Basin.

Detrital zircon populations comprised in the Rio Fresco are rather diverse (Fig. 9C) and include one population originating from the Bacajá Domain (component 1; Table 4, Fig. 9C). Although not representing a major population (contribution of 9%), the presence of this population has potential important implications regarding the age of the Rio Fresco Group, because it requires a connection between the Carajás and the Bacajá domains. The age of the collision between these two domains is generally considered to have occurred around 2.1 Ga (Macambira et al., 2009; Tavares et al., 2018, but see Motta et al., 2019, for an alternative). Assuming a 2.1 Ga collision between the Bacajá and the Carajás domains would imply a depositional age for the Rio Fresco Group younger than 2.1 Ga, during the end of the Rhyacian or the Orosirian (Fig. 10A), in agreement with previous suggestions based on geochemical evidence pointing to deposition younger than the Great Oxidation Event, which occurred between 2.45 Ga and 2.2 Ga (Fabre et al., 2011; Bühn et al., 2012).

The cumulative zircon age distribution given by the bulk detrital zircon population of the Rio Fresco Group suggests an intracontinental setting (Fig. 12). Although potential pitfalls to the tectonic discrimination diagram of Cawood et al. (2012) raised for the Igarapé Bahia Group also apply for the Rio Fresco Group, a bias toward convergent or collisional settings is unlikely given the important time-lag between crystallization and depositional ages for the Rio Fresco Group (Fig. 12). Thus, the Rio Fresco Group could either correspond to a rift, an intracratonic or a pull apart basin (e.g., Cawood et al., 2012). The Rio Fresco Group is related to various other sedimentary units deposited in the Bacajá Domain, such as the Buritirama Formation (Peters et al., 1977) as well as in the Rio Maria Domain, such as the Fazenda São Roque, Cachoeirinha, Tocandera and Rio Naja formations (Vasquez et al., 2008). The large spatial distribution of the Rio Fresco and related sedimentary units (Fig. 3A) points toward an intracratonic basin rather than a small pull apart or rift basin. An intracratonic setting would contradict a previous interpretation suggesting that the Carajás Basin was in a foreland setting during the deposition of the Rio Fresco Group (Tavares et al., 2018; Araújo Filho et al., 2020), but is at odds with the deposition of these sediments during the building of the Transamazonian mountain belt during the Rhyacian (Hurley et al., 1967; Machado et al., 1996; Alkmim and Marshak, 1998; Santos et al., 2000; Cutts et al., 2018, 2019; Moreira et al., 2018; Rossignol et al., 2020b). However, the Carajás Domain was not strongly affected by the Transamazonian orogeny (Machado et al., 1991; Santos et al., 2000). Limited deformation as well as the lack of detrital zircon sourced by the Transamazonian mountain belt suggests that the Carajás Basin was in a rather remote position with respect to the belt. Two different hypotheses can be proposed to account for these observations, implying or not an indirect role of the Transamazonian orogeny. In the first hypothesis, the intracontinental setting suggested by the cumulative distribution of the bulk zircon population (Fig. 11) can be reconciled with a foreland setting if the Carajás was located in a back-bulge area with respect to the Transamazonian mountain belt (Fig. 14). Such a back-bulge basin implies long wavelength flexure of the lithosphere resulting from the Transamazonian collision. The second hypothesis implies a long wavelength flexure of the lithosphere resulting from thermal subsidence, forming a sag basin. A test to these hypotheses can be done by assessing the duration of sedimentation under these tectonic regimes: a rather short lifetime can be expected for a back-bulge basin, while basins sustained by thermal subsidence commonly remain active for hundreds of millions of years. Our present knowledge of the age of the Rio Fresco Group does not allow to decide in favor of one or the other hypothesis.

6. Conclusions

Sedimentary units preserved in the Carajás Domain, southeastern Amazonia Craton, contain unique archives documenting the evolving nature of the South American lithosphere of one of the world's largest cratonic areas from the Eoarchean to the Paleoproterozoic (Fig. 10G). Some uncertainties remain concerning the tectonic setting of the Carajás Basin during the end of the Paleoproterozoic, when the Carajás Basin was in an intracratonic setting and received the products of the erosion of the Amazonia Craton interior. Because the Carajás Basin was located in the hinterland of the Transamazonian mountain belt at that time (around 2.1 Ga), the Carajás Basin could have formed either as a back-bulge basin insulated from direct Transamazonian sedimentary influxes or as a sag basin related to the thermal subsidence of the southeast Amazonian lithosphere.

Beyond these uncertainties, detrital zircon grains from the Neoarchean and early Paleoproterozoic sedimentary archives of the Carajás Basin shed a new light on the early evolution of the Amazonia Craton. The oldest archives, represented by a few ca. 3.6 Ga detrital zircon grains, attest that the geological roots of the Amazonia Craton comprise Eoarchean crust, which is no longer exposed or has not yet been identified. Later, during the Paleoarchean or the early Mesoarchean (<3.1 Ga), the Carajás Domain hosted the oldest documented basin on South America. The occurrence of such a basin, probably corresponding to a greenstone belt, shows that the nucleus of the Carajás Domain was large and rigid enough to sustain the formation and preservation of significant sedimentary units referred to as the Rio Novo Group. During the Neoarchean, at ca. 2.7 Ga, the Parauapebas Large Igneous Province probably covered a large part of the eastern Amazonia Craton and was associated with the deposition of some of the world largest iron deposits. The emplacement of this LIP immediately preceded a continental extensional phase that formed a rift basin infilled by iron formations. With time, iron deposits were progressively replaced by terrigenous sediments, reflecting the development of significant subaerial topography and subsequent erosion of the hinterland of the Amazonia Craton that brought terrigenous influx into the basin. On a global scale, the age of the rifting event in the southeastern Amazonia Craton broadly coincides in time with the break-up of one of the first documented supercontinents, suggesting that the Amazonia Craton could have been part of a large continental landmass during the Neoarchean.

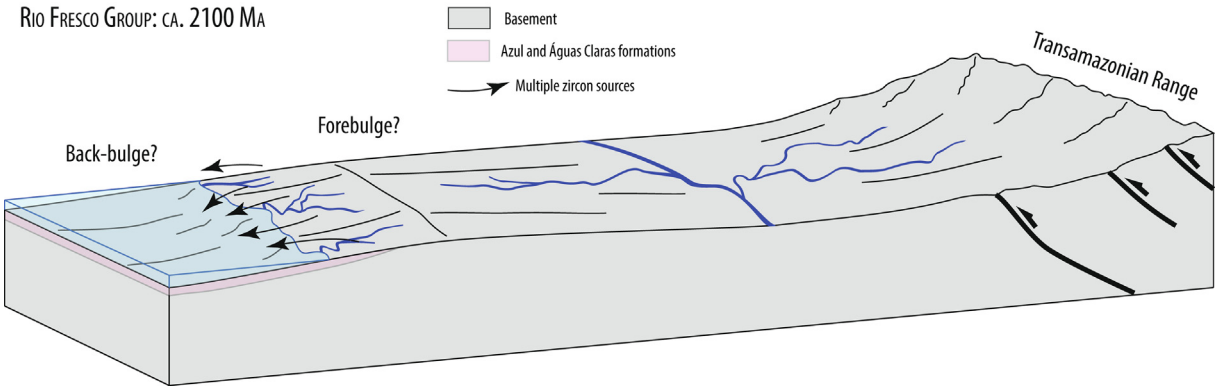

Fig. 14. Tentative reconstruction of the Carajás Basin during the deposition of the Rio Fresco Group.

CRediT authorship contribution statement

Camille Rossignol: Conceptualization, Formal analysis, Investigation, Visualization. **Paul Yves Jean Antonio:** Conceptualization, Investigation. **Francesco Narduzzi:** Investigation. **Eric Siciliano Rego:** Investigation. **Lívia Teixeira:** Investigation. **Romário Almeida de Souza:** Investigation. **Janaína N. Ávila:** Investigation. **Marco A.L. Silva:** Formal analysis, Investigation, Resources. **Cristiano Lana:** Formal analysis, Investigation, Resources. **Ricardo I. F. Trindade:** Project administration, Funding acquisition. **Pascal Philippot:** Conceptualization, Investigation, Project administration, Funding acquisition, Supervision.

Declaration of Competing Interest

The authors declare that they have no known competing financial interests or personal relationships that could have appeared to influence the work reported in this paper.

Acknowledgements

This research was funded by grants of the Fundação Amparo à Pesquisa do Estado de São Paulo (FAPESP; 2015/16235-2, 2017/18840-6, 2018/02645-2, 2018/14617-3, 2018/05892-0, 2019/17732-0, 2019/16066-7 and 2019/12132-5), the Conselho Nacional de Desenvolvimento Científico e Tecnológico (CNPq; 308045/2013-0 and 307353/2019-2), and the Fundação Amparo à Pesquisa do Minas Gerais (FAPEMIG project APQ-03793-16). J. Pereira, D. Vasconcelos, A. Mazoz and A. Alkmim (Universidade Federal de Ouro Preto) are acknowledged for assistance during sample preparation and data acquisition. We thank S. Huhn (Vale) for making available the drill cores intercepting the Azul Formation. Cathodoluminescence images of the zircon grains analyzed during this study were obtained by the Microscopy and Microanalysis Laboratory (LMic) of the Universidade Federal de Ouro Preto, a member of the Microscopy and Microanalysis Network of Minas Gerais State/Brazil/FAPEMIG. We acknowledge David Chew and two anonymous reviewers for constructive comments that helped to clarify and improve the manuscript.

Data Availability

Datasets related to this article can be found at http://dx.doi.org/10.17632/tr75ph44gs.1, an open-source online data repository hosted at Mendeley Data. It comprises 6 appendices, as follow: Appendix 1. U-Pb detrital zircon grains dataset; Appendix 2. Analytical methods for U-Pb dating on zircon grains; Appendix 3. Bayes Mix parameters; Appendix 4. Analytical results for U-Pb dating on zircon grains from dykes crosscutting the Rio Novo Group; Appendix 5. Analytical results for U-Pb dating on zircon grains from the Azul Formation; Appendix 6. Complementary geochronological diagrams.

References

Abbott, D.H., Isley, A.E., 2002. The instensity, occurrence, and duration of superplume events and eras over geological time. J. Geodyn. 34, 265–307. https://doi.org/10.1016/S0264-3707(02)00024-8.

Alkmim, F., Marshak, S., 1998. Transamazonian Orogeny in the Southern São Francisco Craton Region, Minas Gerais, Brazil: evidence for Paleoproterozoic collision and collapse in the Quadrilatero Ferrifero. Precambrian Res. 90, 29–58. https://doi.org/10.1016/S0301-9268(98)00032-1.

Almeida, J.A.C., Dall'Agnol, R., Leite, A.A.S., 2013. Geochemistry and zircon geochronology of the Archean granite suites of the Rio Maria granite-greenstone terrane, Carajás Province. Brazil. J. South Am. Earth Sci. 42, 103–126. https://doi.org/10.1016/j.jsames.2012.10.008.

Althoff, F., Barbey, P., Boullier, A.M., 2014. 2.8-3.0 Ga plutonism and deformation in the SE Amazonian craton: The Archaean granitoids of Marajoara (Carajas Mineral Province, Brazil). Precambrian Res. 104, 187–206. https://doi.org/10.1016/S0301-9268(00)00103-0.

Amidon, W.H., Burbank, D.W., Gehrels, G.E., 2005. Construction of detrital mineral populations: insights from mixing of U-Pb zircon ages in Himalayan rivers. Basin Res. 17, 463–485. https://doi.org/10.1111/j.1365-2117.2005.00279.x.

Andersen, T., 2005. Detrital zircons as tracers of sedimentary provenance: limiting conditions from statistics and numerical simulation. Chem. Geol., 249–270 https://doi.org/10.1016/j.chemgeo.2004.11.013.

Antonio, P.Y.J., D'Agrella-Filho, M.S., Nédélec, A., Poujol, M., Sanchez, C., Dantas, E.L., Dall'Agnol, R., Teixeira, M.F.B., Proietti, A., Martínez Dopico, C.I., Oliveira, D.C., Silva, F.F., Marangoanha, B., Trindade, R.I.F., 2021. New constraints for paleogeographic reconstructions at ca. 1.88 Ga from geochronology and paleomagnetism of the Carajás dyke swarm (eastern Amazonia). Precambrian Res. 353. https://doi.org/10.1016/j.precamres.2020.106039.

Antonio, P.Y.J., D'Agrella-Filho, M.S., Trindade, R.I.F., Nédélec, A., de Oliveira, D.C., da Silva, F.F., Roverato, M., Lana, C., 2017. Turmoil before the boring billion: Paleomagnetism of the 1880–1860 Ma Uatumã event in the Amazonian craton. Gondwana Res. 49, 106–129. https://doi.org/10.1016/j.gr.2017.05.006.

Araújo Filho, R.C., Nogueira, A.C.R., Araújo, R.N., 2020. New stratigraphic proposal of a paleoproterozoic siliciclastic succession: Implications for the evolution of the Carajás basin, amazonian craton. Brazil. J. South Am. Earth Sci. 102665. https://doi.org/10.1016/j.jsames.2020.102665.

Araujo, O.J.B., Maia, R.G.N., 1991. Serra dos Carajás Folha SB.22-Z-A - Estado do Pará. Texto explicativo (in Portuguese).

Araujo, R., Nogueira, A., 2019. Serra sul diamictite of the carajas basin (Brazil): A paleoproterozoic glaciation on the amazonian craton. Geology 47, 1166–1170. https://doi.org/10.1130/G46923.1.

Baratoux, L., Metelka, V., Naba, S., Jessell, M.W., Grégoire, M., Ganne, J., 2011. Juvenile Paleoproterozoic crust evolution during the Eburnean orogeny (~2.2-2.0 Ga), western Burkina Faso. Precambrian Res. 191, 18–45. https://doi.org/10.1016/j.precamres.2011.08.010.

Barley, M.E., Bekker, A., Krapez, B., 2005. Late Archean to Early Paleoproterozoic global tectonics, environmental change and the rise of atmospheric oxygen. Earth Planet. Sci. Lett. 238, 156–171. https://doi.org/10.1016/j.epsl.2005.06.062.

Barley, M.E., Pickard, A.L., Sylvester, P.J., 1997. Emplacement of a large igenous province as a possible cause of banded iron formation 2.45 billion years ago. Nature 385, 55–58.

Barros, C.E.M., Sardinha, A.S., Barbosa, J.P.O., MacAmbira, M.J.B., Barbey, P., Boullier, A.M., 2009. Structure, petrology, geochemistry and zircon U/Pb and Pb/Pb geochronology of the synkinematic Archean (2.7 Ga) A-type granites from the

Carajas metallogenic province, northern Brazil. Can. Mineral. 47, 1423–1440. https://doi.org/10.3749/canmin.47.6.1423.

Bauer, A.B., Reimink, J.R., Chacko, T., Foley, B.J., Shirey, S.B., Pearson, D.G., 2020. Hafnium isotopes in zircons document the gradual onset of mobile-lid tectonics. Geochemical Perspect. Lett. 1–6. https://doi.org/10.7185/geochemlet.2015.

Bédard, J.H., 2018. Stagnant lids and mantle overturns: Implications for Archaean tectonics, magmagenesis, crustal growth, mantle evolution, and the start of plate tectonics. Geosci. Front. 9, 19–49. https://doi.org/10.1016/j.gsf.2017.01.005.

Beisiegel, V.D.R., Bernardelli, A.L., Drummond, N.F., Ruff, A.W., Tremaine, J.W.R., 1973. Geologia e Recursos Minerais da Serra dos Carajás. Rev. Bras. Geociências 3, 215–242.

Bekker, A., Slack, J.F., Planavsky, N.J., Krapež, B., Hofmann, A., Konhauser, K.O., Rouxel, O., 2010. Iron formation: The sedimentary product of a complex interplay among mantle, tectonic, oceanic, and biospheric processes. Econ. Geol. 105, 467–508. https://doi.org/10.2113/gsecongeo.105.3.467.

Berni, G.V., Heinrich, C.A., Lobato, L.M., Wall, V.J., Rosière, C.A., Freitas, M.A., 2014. The Serra Pelada Au-Pd-Pt deposit, Carajás, Brazil: Geochemistry, mineralogy, and zoning of hydrothermal alteration. Econ. Geol. 109, 1883–1899. https://doi.org/10.2113/econgeo.109.7.1883.

Bertrand, J.-M., Jardim de Sa, E.M., 1990. Where are the Eburnian-Transamazonian collisional belts?. Can. J. Earth Sci. 27, 1382–1393.

Bindeman, I.N., Zakharov, D.O., Palandri, J., Greber, N.D., Dauphas, N., Retallack, G.J., Hofmann, A., Lackey, J.S., Bekker, A., 2018. Rapid emergence of subaerial landmasses and onset of a modern hydrologic cycle 2.5 billion years ago. Nature 557, 545–548. https://doi.org/10.1038/s41586-018-0131-1.

Bryan, S.E., Ernst, R.E., 2008. Revised definition of Large Igneous Provinces (LIPs). Earth-Science Rev. 86, 175–202. https://doi.org/10.1016/j.earscirev.2007.08.008.

Bühn, B., Santos, R.V., Dardenne, M.A., de Oliveira, C.G., 2012. Mass-dependent and mass-independent sulfur isotope fractionation (δ34S and δ33S) from Brazilian Archean and Proterozoic sulfide deposits by laser ablation multi-collector ICP-MS. Chem. Geol. 312–313, 163–176. https://doi.org/10.1016/j.chemgeo.2012.04.003.

Cabral, A.R., Bühn, B., Seabra Gomes, A.A., Galbiatti, H.F., Lehmann, B., Halder, S., 2017. Multiple sulfur isotopes from the Neoarchaean Serra Sul black shale, Carajás mineral province, northern Brazil. J. South Am. Earth Sci. 79, 377–383. https://doi.org/10.1016/j.jsames.2017.08.002.

Cabral, A.R., Burgess, R., Lehmann, B., 2011. Late Cretaceous bonanza-style metal enrichment in the Serra Pelada Au-Pd-Pt deposit, pará. Brazil. Econ. Geol. 106, 119–125. https://doi.org/10.2113/econgeo.106.1.119.

Cabral, A.R., Creaser, R.A., Nägler, T., Lehmann, B., Voegelin, A.R., Belyatsky, B., Pašava, J., Seabra Gomes, A.A., Galbiatti, H., Böttcher, M.E., Escher, P., 2013. Trace-element and multi-isotope geochemistry of Late-Archean black shales in the Carajás iron-ore district. Brazil. Chem. Geol. 362, 91–104. https://doi.org/10.1016/j.chemgeo.2013.08.041.

Cabral, A.R., Riehl, W., 2020. Comments on "Critical assessment of geochronological data from the Carajás Mineral Province, Brazil: implications for metallogeny and tectonic evolution." Ore Geol. Rev. https://doi.org/10.1016/j.oregeorev.2020.103722

Campbell, I.H., 2005. Large igneous provinces and the mantle plume hypothesis. Elements 1, 265–269. https://doi.org/10.2113/gselements.1.5.265.

Cawood, P.A., Hawkesworth, C.J., Dhuime, B., 2012. Detrital zircon record and tectonic setting. Geology 40, 875–878. https://doi.org/10.1130/G32945.1.

Cohen, K., Finney, S., Gibbard, P., Fan, J., 2013. The ICS International Chronostratigraphic Chart. Episodes 36, 199–204.

Compston, W., Gallagher, K., 2012. New SHRIMP zircon ages from tuffs within the British Palaeozoic stratotypes. Gondwana Res. 21, 719–727. https://doi.org/10.1016/j.gr.2011.11.010.

Cordani, U.G., Ramos, V.A., Fraga, L.M., Cegarra, M., Delgado, I., de Souza, K.G., Gomes, F.E.M., Schobbenhaus, C., 2016. Tectonic map of South America at 1:5.9M. Scale 15,900,000 CGMW-CPRM-.

Cordani, U.G., Teixeira, W., 2007. Proterozoic accretionary belts in the Amazonian Craton. Mem. Geol. Soc. Am. 200, 297–320. https://doi.org/10.1130/2007.1200(14).

Cordani, U.G., Teixeira, W., D'Agrella-Filho, M.S., Trindade, R.I., 2009. The position of the Amazonian Craton in supercontinents. Gondwana Res. 15, 396–407. https://doi.org/10.1016/j.gr.2008.12.005.

Corfu, F., Hanchar, J.M., Hoskin, P.W.O., Kinny, P., 2003. Atlas of Zircon Textures. In: Hanchar, J.M., Hoskin, P.W.O. (Eds.), Zircon. Mineralogical Society of America and Geochemical Society, Washington, DC, United States, pp. 469–500.

Coutts, D.S., Matthews, W.A., Hubbard, S.M., 2019. Assessment of widely used methods to derive depositional ages from detrital zircon populations. Geosci. Front. 10, 1421–1435. https://doi.org/10.1016/j.gsf.2018.11.002.

Cox, K.G., 1989. The role of mantle plumes in the development of continental drainage patterns. Nature 342, 873–877. https://doi.org/10.1038/340301a0.

Crowley, Q., Heron, K., Riggs, N., Kamber, B., Chew, D., McConnell, B., Benn, K., 2014. Chemical Abrasion Applied to LA-ICP-MS U-Pb Zircon Geochronology. Minerals 4, 503–518. https://doi.org/10.3390/min4020503.

Cutts, K., Lana, C., Alkmim, F., Farina, F., Moreira, H., Coelho, V., 2019. Metamorphism and exhumation of basement gneiss domes in the Quadrilátero Ferrífero: Two stage dome-and-keel evolution? Geosci. Front. 10, 1765–1787. https://doi.org/10.1016/j.gsf.2019.02.009.

Cutts, K., Lana, C., Alkmim, F., Peres, G.G., 2018. Metamorphic imprints on units of the southern Araçuaí belt, SE Brazil: The history of superimposed Transamazonian and Brasiliano orogenesis. Gondwana Res. 58, 211–234. https://doi.org/10.1016/j.gr.2018.02.016.

Dall'Agnol, R., Cunha, I.R.V., Guimarães, F.V., Oliveira, D.C., Teixeira, M.F.B., Feio, G.R.L., Lamarão, C.N., 2017. Mineralogy, geochemistry, and petrology of Neoarchean ferroan to magnesian granites of Carajás Province, Amazonian Craton: The origin of hydrated granites associated with charnockites. Lithos 277, 3–32. https://doi.org/10.1016/j.lithos.2016.09.032.

Dall'Agnol, R., Teixeira, N.P., Rämö, O.T., Moura, C.A.V., Macambira, M.J.B., de Oliveira, D.C., 2005. Petrogenesis of the Paleoproterozoic rapakivi A-type granites of the Archean Carajás metallogenic province, Brazil. Lithos 80, 101–129. https://doi.org/10.1016/j.lithos.2004.03.058.

Dalstra, H., Guedes, S., 2004. Giant hydrothermal hematite deposits with Mg-Fe metasomatism: A comparison of the Carajás, Hamersley, and other iron ores. Econ. Geol. 99, 1793–1800. https://doi.org/10.2113/gsecongeo.99.8.1793.

Dardenne, M.A., Ferreira Filho, C.F., Meirelles, M.R., 1988. The role of shoshonitic and calc-alkaline suites in the tectonic evolution of the Carajás District. Brazil. J. South Am. Earth Sci. 1, 363–372. https://doi.org/10.1016/0895-9811(88)90023-5.

de Almeida, F.F.M., Brito Neves, B.B., Carneiro, C.D.R., 2000. The origin and evolution of the South American Platform. Earth-Science Rev. 50, 77–111. https://doi.org/10.1016/S0012-8252(99)00072-0.

de Saint Blanquat, M., Horsman, E., Habert, G., Morgan, S., Vanderhaeghe, O., Law, R., Tikoff, B., 2011. Multiscale magmatic cyclicity, duration of pluton construction, and the paradoxical relationship between tectonism and plutonism in continental arcs. Tectonophysics 500, 20–33. https://doi.org/10.1016/j.tecto.2009.12.009.

Dickinson, W.R., Gehrels, G.E., 2009. Use of U-Pb ages of detrital zircons to infer maximum depositional ages of strata: A test against a Colorado Plateau Mesozoic database. Earth Planet. Sci. Lett. 288, 115–125. https://doi.org/10.1016/j.epsl.2009.09.013.

Dreher, A.M., Xavier, R.P., Martini, S.L., 2005. Fragmental rocks if the Igarape Bahia Cu-Au deposits, Carajas minaral Province. Brazil. Rev. Bras. Geociências 35, 359–368.

Dreher, A.M., Xavier, R.P., Taylor, B.E., Martini, S.L., 2008. New geologic, fluid inclusion and stable isotope studies on the controversial Igarapé Bahia Cu-Au deposit, Carajás Province. Brazil. Miner. Depos. 43, 161–184. https://doi.org/10.1007/s00126-007-0150-6.

Eriksson, P.G., Catuneanu, O., Sarkar, S., Tirsgaard, H., 2005. Patterns of sedimentation in the Precambrian. Sediment. Geol. 176, 17–42. https://doi.org/10.1016/j.sedgeo.2005.01.003.

Eriksson, P.G., Condie, K.C., 2014. Cratonic sedimentation regimes in the ca. 2450–2000Ma period: Relationship to a possible widespread magmatic slowdown on Earth?. Gondwana Res. 25, 30–47. https://doi.org/10.1016/j.gr.2012.08.005.

Ernst, W.G., 2009. Archean plate tectonics, rise of Proterozoic supercontinentality and onset of regional, episodic stagnant-lid behavior. Gondwana Res. 15, 243–253. https://doi.org/10.1016/j.gr.2008.06.010.

Fabre, S., Nédélec, A., Poitrasson, F., Strauss, H., Thomazo, C., Nogueira, A., 2011. Iron and sulphur isotopes from the Carajás mining province (Pará, Brazil): Implications for the oxidation of the ocean and the atmosphere across the Archaean-Proterozoic transition. Chem. Geol. 289, 124–139. https://doi.org/10.1016/j.chemgeo.2011.07.019.

Fedo, C.M., Sircombe, K.N., Rainbird, R.H., 2003. Detrital Zircon Analysis of the Sedimentary Record. In: Hanchar, J.M., Hoskin, P.W.O. (Eds.), Zircon. Mineralogical Society of America and Geochemical Society, Washington, DC, United States, pp. 277–303.

Feio, G.R.L., Dall'Agnol, R., Dantas, E.L., Macambira, M.J.B., Gomes, A.C.B., Sardinha, A. S., Oliveira, D.C., Santos, R.D., Santos, P.A., 2012. Geochemistry, geochronology, and origin of the Neoarchean Planalto Granite suite, Carajás, Amazonian craton: A-type or hydrated charnockitic granites?. Lithos 151, 57–73. https://doi.org/10.1016/j.lithos.2012.02.020.

Figueiredo e Silva, R.C., Lobato, L.M., Rosière, C.A., Hagemann, S., Zucchetti, M., Baars, F.J., Morais, R., Andrade, I., 2008. A Hydrothermal Origin for the Jaspilite-Hosted, Giant Serra Norte Iron Ore Deposits in the Carajás Mineral Province, Pará State, Brazil, in: Hagemann, S., Rosière, C.A., Gutzmer, J., Beukes, N.J. (Eds.), Banded Iron Formation-Related High-Grade Iron Ore. Society of Economic Geologists, pp. 255–290. https://doi.org/10.5382/rev.15.10

Feio, G.R.L., Dall'Agnol, R., Dantas, E.L., Macambira, M.J.B., Santos, J.O.S., Althoff, F.J., Soares, J.E.B., 2013. Archean granitoid magmatism in the Canaã dos Carajás area: Implications for crustal evolution of the Carajás province, Amazonian craton, Brazil. Precambrian Res. 227, 157–185. https://doi.org/10.1016/j.precamres.2012.04.007.

Flament, N., Coltice, N., Rey, P.F., 2008. A case for late-Archaean continental emergence from thermal evolution models and hypsometry. Earth Planet. Sci. Lett. 275, 326–336. https://doi.org/10.1016/j.epsl.2008.08.029.

Galarza, M.A., Macambira, M.J.B., Villas, R.N., 2008. Dating and isotopic characteristics (Pb and S) of the Fe oxide-Cu-Au-U-REE Igarapé Bahia ore deposit, Carajás mineral province, Pará state. Brazil. J. South Am. Earth Sci. 25, 377–397. https://doi.org/10.1016/j.jsames.2007.07.006.

Gallagher, K., Charvin, K., Nielsen, S., Sambridge, M., Stephenson, J., 2009. Markov chain Monte Carlo (MCMC) sampling methods to determine optimal models, model resolution and model choice for Earth Science problems. Mar. Pet. Geol. 26, 525–535. https://doi.org/10.1016/j.marpetgeo.2009.01.003.

Gawthorpe, R.L., Leeder, M.R., 2000. Tectono-sedimentary evolution of active extensional basins. Basin Res. 12, 195–218. https://doi.org/10.1111/j.1365-2117.2000.00121.x.

Gehrels, G.E., 2014. Detrital Zircon U-Pb Geochronology Applied to Tectonics. Annu. Rev. Earth Planet. Sci. 42, 127–149. https://doi.org/10.1146/annurev-earth-050212-124012.

Gibbs, A.K., Wirth, K.R., Hirata, W.K., Olszewski Jr, W.J., 1986. Age and composition of the Grão Pará groups volcanics. Serra dos Carajás. Rev. Bras. Geociências 16, 201–211.

Grainger, C.J., Groves, D.I., Tallarico, F.H.B., Fletcher, I.R., 2008. Metallogenesis of the Carajás Mineral Province, Southern Amazon Craton, Brazil: Varying styles of Archean through Paleoproterozoic to Neoproterozoic base- and precious-metal mineralisation. Ore Geol. Rev. 33, 451–489. https://doi.org/10.1016/j.oregeorev.2006.10.010.

Gumsley, A.P., Chamberlain, K.R., Bleeker, W., Soderlund, U., De Kock, M.O., Larsson, E.R., 2017. Timing and tempo of the Great Oxidation Event. Proc. Natl. Acad. Sci. 114, 1811–1816. https://doi.org/10.1073/pnas.1608824114.

Hagemann, S.G., Angerer, T., Duuring, P., Rosière, C.A., Figueiredo e Silva, R.C., Lobato, L., Hensler, A.S., Walde, D.H.G., 2016. BIF-hosted iron mineral system: A review. Ore Geol. Rev. 76, 317–359. https://doi.org/10.1016/j.oregeorev.2015.11.004.

Hietpas, J., Samson, S., Moecher, D., Chakraborty, S., 2011. Enhancing tectonic and provenance information from detrital zircon studies: assessing terrane-scale sampling and grain-scale characterization. J. Geol. Soc. London. 168, 309–318. https://doi.org/10.1144/0016-76492009-163.

Hill, R.I., 1991. Starting plumes and continental break-up. Earth Planet. Sci. Lett. 104, 398–416. https://doi.org/10.1016/0012-821X(91)90218-7.

Hirata, W.K., Rigon, J.C., Kadekaru, K., Cordeiro, A.A.C., Meirelles, E.M., 1982. Geologia regional da Província Mineral de Carajás, in: Anais Do Simpósio de Geologia Da Amazônia. Sociedade Brasileira de Geologia - Núcleo Norte, Belém, pp. 100–110 (in Portuguese).

Hurley, P.M., De Almeida, F.F.M., Melcher, G.C., Cordani, U.G., Rand, J.R., Kawashita, K., Vandoros, P., Pinson, W.H., Fairbairn, H.W., 1967. Test of continental drift by comparison of radiometric ages. Science 157 (3788), 495–500. https://doi.org/10.1126/science.157.3788.495.

Huyskens, M.H., Zink, S., Amelin, Y., 2016. Evaluation of temperature-time conditions for the chemical abrasion treatment of single zircons for U-Pb geochronology. Chem. Geol. 438, 25–35. https://doi.org/10.1016/j.chemgeo.2016.05.013.

Isley, A.E., Abbott, D.H., 1999. Plume-related mafic volcanism and the deposition of banded iron formation. J. Geophys. Res. Solid Earth 104, 15461–15477. https://doi.org/10.1029/1999jb900066.

Jackson, S.E., Pearson, N.J., Griffin, W.L., Belousova, E.A., 2004. The application of laser ablation-inductively coupled plasma-mass spectrometry to in situ U-Pb zircon geochronology. Chem. Geol. 211, 47–69. https://doi.org/10.1016/j.chemgeo.2004.06.017.

Jasra, A., Stephens, D.A., Gallagher, K., Holmes, C.C., 2006. Bayesian Mixture Modelling in Geochronology via Markov Chain Monte Carlo. Math. Geol. 38, 269–300. https://doi.org/10.1007/s11004-005-9019-3.

Klein, C., Ladeira, E.A., 2002. Petrography and Geochemistry of the Least Altered Banded Iron-Formation of the Archean Carajas Formation, Northern Brazil. Econ. Geol. 97, 643–651. https://doi.org/10.2113/97.3.643.

Košler, J., Sláma, J., Belousova, E., Corfu, F., Gehrels, G.E., Gerdes, A., Horstwood, M.S. A., Sircombe, K.N., Sylvester, P.J., Tiepolo, M., Whitehouse, M.J., Woodhead, J.D., 2013. U-Pb Detrital Zircon Analysis - Results of an Inter-laboratory Comparison. Geostand. Geoanalytical Res. 37, 243–259. https://doi.org/10.1111/j.1751-908X.2013.00245.x.

Košler, J., Sylvester, P.J., 2003. Present Trends and the Future of Zircon in Geochronology: Laser Ablation ICPMS. In: Hanchar, J.M., Hoskin, P.W.O. (Eds.), Zircon. Mineralogical Society of America and Geochemical Society, Washington, DC, United States, pp. 243–275.

Krymsky, R.S., Macambira, M.J.B., Lafon, J.-M., Estumano, G.S., 2007. Uranium-lead dating method at the Pará-Iso isotope geology laboratory, UFPA, Belém - Brazil. Brazil. An. Acad. Bras. Cienc. 79, 115–128. https://doi.org/10.1590/S0001-37652007000100014.

Kumar, A., Parashuramulu, V., Shankar, R., Besse, J., 2017. Evidence for a Neoarchean LIP in the Singhbhum craton, eastern India: Implications to Vaalbara supercontinent. Precambrian Res. 292, 163–174. https://doi.org/10.1016/j.precamres.2017.01.018.

Kump, L.R., Barley, M.E., 2007. Increased subaerial volcanism and the rise of atmospheric oxygen 2.5 billion years ago. Nature 448, 1033–1036. https://doi.org/10.1038/nature06058.

Lacasse, C.M., Ganade, C.E., Mathieu, L., Teixeira, N.A., Lopes, L.B.L., Monteiro, C.F., 2020. Restoring original composition of hydrothermally altered Archean metavolcanic rocks of the Carajás Mineral Province (Brazil): Geodynamic implications for the transition from lid to mobile tectonics. Lithos 372–373,. https://doi.org/10.1016/j.lithos.2020.105647 105647.

Lawrence, R.L., Cox, R., Mapes, R.W., Coleman, D.S., 2011. Hydrodynamic fractionation of zircon age populations. Geol. Soc. Am. Bull. 123, 295–305. https://doi.org/10.1130/B30151.1.

Licht, A., Pullen, A., Kapp, P., Abell, J., Giesler, N., 2016. Eolian cannibalism: Reworked loess and fluvial sediment as the main sources of the Chinese Loess Plateau. Geol. Soc. Am. Bull. 128, 944–956. https://doi.org/10.1130/B31375.1.

Lindenmayer, Z.G., Laux, J.H., Teixeira, J.B.G., 2001. Concidarações sobre a origem das formações ferríferas da Formação Carajás, Serra dos Carajás. Rev. Bras. Geociências 31, 21–28. https://doi.org/10.25249/0375-7536.20013112128. (in Portuguese).

Ludwig, K.R., 2012. User's Manual for a geochronological toolkit for Microsoft Excel. Berkeley Geochronological Cent. 75.

Ludwig, K.R., 1998. On the Treatment of Concordant Uranium-Lead Ages. Geochim. Cosmochim. Acta 62, 665–676. https://doi.org/10.1016/S0016-7037(98)00059-3.

Macambira, M.J.B., Lancelot, J.R., 1996. Time constraints for the formation of the Archean Rio Maria crust, southeastern Amazonian Craton. Brazil. Int. Geol. Rev. 38, 1134–1142. https://doi.org/10.1080/00206819709465386.

Macambira, M.J.B., Schrank, A., 2002. Químio-estratigrafia e evolução dos jaspilitos da Formação Carajás (PA). Rev. Bras. Geociências 32, 567–578. https://doi.org/10.25249/0375-7536.2002324567578 (in Portuguese).

Macambira, M.J.B., Vasquez, M.L., Silva, D.C.C., Galarza, M.A., Barros, C.E.M., Camelo, J.F., 2009. Crustal growth of the central-eastern Paleoproterozoic domain, SW Amazonian craton: Juvenile accretion vs. reworking. J. South Am. Earth Sci. 27, 235–246. https://doi.org/10.1016/j.jsames.2009.02.001.

Machado, N., Lindenmayer, Z., Krogh, T.E., Lindenmayer, D., 1991. U-Pb geochronology of Archean magmatism and basement reactivation in the Carajás area, Amazon shield. Brazil. Precambrian Res. 49, 329–354. https://doi.org/10.1016/0301-9268(91)90040-H.

Machado, N., Schrank, A., Noce, C.M., Gauthier, G., 1996. Ages of detrital zircon from Archean-Paleoproterozoic sequences: Implications for Greenstone Belt setting and evolution of a Transamazonian foreland basin in Quadrilátero Ferrífero, southeast Brazil. Earth Planet. Sci. Lett. 141, 259–276. https://doi.org/10.1016/0012-821X(96)00054-4.

Mansur, E.T., Ferreira Filho, C.F., 2016. Magmatic structure and geochemistry of the Luanga Mafic-Ultramafic Complex: Further constraints for the PGE-mineralized magmatism in Carajás, Brazil. Lithos 266–267, 28–43. https://doi.org/10.1016/j.lithos.2016.09.036.

Markwitz, V., Kirkland, C.L., 2018. Source to sink zircon grain shape: Constraints on selective preservation and significance for Western Australian Proterozoic basin provenance. Geosci. Front. 9, 431–439. https://doi.org/10.1016/j.gsf.2017.04.004.

Martins, P.L.G., Toledo, C.L.B., Silva, A.M., Chemale, F., Santos, J.O.S., Assis, L.M., 2017. Neoarchean magmatism in the southeastern Amazonian Craton, Brazil: Petrography, geochemistry and tectonic significance of basalts from the Carajás Basin. Precambrian Res. 302, 340–357. https://doi.org/10.1016/j.precamres.2017.10.013.

Melo, G.H.C., Monteiro, L.V.S., Xavier, R.P., Moreto, C.P.N., Arquaz, R.M., Silva, M.A.D., 2019. Evolution of the Igarapé Bahia Cu-Au deposit, Carajás Province (Brazil): Early syngenetic chalcopyrite overprinted by IOCG mineralization. Ore Geol. Rev. 111,. https://doi.org/10.1016/j.oregeorev.2019.102993 102993.

Melo, G.H.C., Monteiro, L.V.S., Xavier, R.P., Moreto, C.P.N., Santiago, E.S.B., Dufrane, S. A., Aires, B., Santos, A.F.F., 2017. Temporal evolution of the giant Salobo IOCG deposit, Carajás Province (Brazil): constraints from paragenesis of hydrothermal alteration and U-Pb geochronology. Miner. Depos. 52, 709–732. https://doi.org/10.1007/s00126-016-0693-5.

Milhomem Neto, J.M., Lafon, J.M., 2019. Zircon U-Pb and Lu-Hf isotope constraints on Archean crustal evolution in Southeastern Guyana Shield. Geosci. Front. 10, 1477–1506. https://doi.org/10.1016/j.gsf.2018.09.012.

Moreira, H., Seixas, L., Storey, C., Fowler, M., Lasalle, S., Stevenson, R., Lana, C., 2018. Evolution of Siderian juvenile crust to Rhyacian high Ba-Sr magmatism in the Mineiro Belt, southern São Francisco Craton. Geosci. Front. 9, 977–995. https://doi.org/10.1016/j.gsf.2018.01.009.

Moreto, C.P.N., Monteiro, L.V.S., Xavier, R.P., Creaser, R.A., DuFrane, S.A., Tassinari, C. C.G., Sato, K., Kemp, A.I.S., Amaral, W.S., 2015. Neoarchean and paleoproterozoic iron oxide-copper-gold events at the sossego deposit, Carajás Province, Brazil: Re-Os and U-Pb geochronological evidence. Econ. Geol. 110, 809–835. https://doi.org/10.2113/econgeo.110.3.809.

Motta, J.G., Souza Filho, C.R., Carranza, E.J.M., Braitenberg, C., 2019. Archean crust and metallogenic zones in the Amazonian Craton sensed by satellite gravity data. Sci. Rep. 9, 2565. https://doi.org/10.1038/s41598-019-39171-9.

Najman, Y., 2006. The detrital record of orogenesis: A review of approaches and techniques used in the Himalayan sedimentary basins. Earth-Science Rev. 74, 1–72. https://doi.org/10.1016/j.earscirev.2005.04.004.

Olszewski, W.J., Wirth, K.R., Gibbs, A.K., Gaudette, H.E., 1989. The age, origin, and tectonics of the Grão Pará Group and associated rocks, Serra dos Carajás, Brazil: Archean continental volcanism and rifting. Precambrian Res. 42, 229–254. https://doi.org/10.1016/0301-9268(89)90013-2.

Parra-Avila, L.A., Baratoux, L., Eglinger, A., Fiorentini, M.L., Block, S., 2019. The Eburnean magmatic evolution across the Baoulé-Mossi domain: Geodynamic implications for the West African Craton. Precambrian Res. 332,. https://doi.org/10.1016/j.precamres.2019.105392 105392.

Pehrsson, S.J., Berman, R.G., Eglington, B., Rainbird, R., 2013. Two Neoarchean supercontinents revisited: The case for a Rae family of cratons. Precambrian Res. 232, 27–43. https://doi.org/10.1016/j.precamres.2013.02.005.

Peters, T.J., Valarelli, J.V., Coutinho, J.M.V., Sommerauer, J., von Raumer, J., 1977. The manganese deposits of Buritirama (Pará , Brazil). Schweizerische Mineral. und Petrogr. Mitteilungen - Bull. suisse minéralogie pétrographie 57, 313–327. https://doi.org/http://dx.doi.org/10.5169/seals-44438 Nutzungsbedingungen

Pidgeon, R.T., MacAmbira, M.J.B., Lafon, J.M., 2000. Th-U-Pb isotopic systems and internal structures of complex zircons from an enderbite from the Pium Complex, Carajas Province, Brazil: Evidence for the ages of granulite facies metamorphism and the protolith of the enderbite. Chem. Geol. 166, 159–171. https://doi.org/10.1016/S0009-2541(99)00190-4.

Pinheiro, R.V.L., Holdsworth, R.E., 1997. Reactivation of Archaean strike-slip fault systems, Amazon region. Brazil. J. Geol. Soc. London. 154, 99–103. https://doi.org/10.1144/gsjgs.154.1.0099.

Pons, M.L., Fujii, T., Rosing, M., Quitté, G., Télouk, P., Albarède, F., 2013. A Zn isotope perspective on the rise of continents. Geobiology 11, 201–214. https://doi.org/10.1111/gbi.12030.

Pullen, A., Ibanez-Mejia, M., Gehrels, G.E., Ibanez-Mejia, J.C., Pecha, M., 2014. What happens when n=1000? Creating large-n geochronological datasets with LA-ICP-MS for geologic investigations. J. Anal. At. Spectrom. 29, 971–980. https://doi.org/10.1039/c4ja00024b.

Rasmussen, B., Bekker, A., Fletcher, I.R., 2013. Correlation of Paleoproterozoic glaciations based on U-Pb zircon ages for tuff beds in the Transvaal and Huronian Supergroups. Earth Planet. Sci. Lett. 382, 173–180. https://doi.org/10.1016/j.epsl.2013.08.037.

Rego, E.S., Busigny, V., Lalonde, S.V., Philippot, P., Bouyon, A., Rossignol, C., Babinski, M., Zapparoli, A., 2021. Anoxygenic photosynthesis linked to Neoarchean iron formations in Carajás (Brazil). Geobiology. https://doi.org/10.1111/gbi.12438. In press.

Requia, K., Stein, H., Fontboté, L., Chiaradia, M., 2003. Re-Os and Pb-Pb geochronology of the Archean Salobo iron oxide copper-gold deposit, Carajás mineral province, northern Brazil. Miner. Depos. 38, 727–738. https://doi.org/10.1007/s00126-003-0364-1.

Rey, P.F., Coltice, N., 2008. Neoarchean lithospheric strengthening and the coupling of Earth's geochemical reservoirs. Geology 36, 635–638. https://doi.org/10.1130/G25031A.1.

Ribeiro da Luz, B., Crowley, J.K., 2012. Morphological and chemical evidence of stromatolitic deposits in the 2.75Ga Carajás banded iron formation. Brazil. Earth Planet. Sci. Lett. 355–356, 60–72. https://doi.org/10.1016/j.epsl.2012.08.028.

Ronov, A.B., 1972. Evolution of Rock Composition and Geochemical Processes in the Sedimentary Shell of the Earth. Sedimentology 19, 157–172. https://doi.org/10.1111/j.1365-3091.1972.tb00019.x.

Ronze, P.C., Soares, A.D.V., Santos, M.G.S., Barreira, C.F., 2000. Alemao copper-gold (U-REE) deposits, Carajas, Brazil, in: Porter, T.M. (Ed.), Hydrothermal Iron Oxide Copper-Gold and Related Deposits: A Global Perspective. PCG Publishing, pp. 191–202.

Rossignol, C., Bourquin, S., Poujol, M., Hallot, E., Dabard, M.-P., Nalpas, T., 2016. The volcaniclastic series from the Luang Prabang Basin, Laos: A witness of a triassic magmatic arc ?. J. Asian Earth Sci. 120, 159–183. https://doi.org/10.1016/j.jseaes.2016.02.001.

Rossignol, C., Rego, E., Narduzzi, F., Teixeira, L., Avila, J.N., Silva, M.A.L., Lana, C., Philippot, P., 2020a. Stratigraphy and geochronological constraints of the Serra Sul Formation (Carajas Basin, Amazonian Craton, Brazil). Precambrian Res. 351,. https://doi.org/10.1016/j.precamres.2020.105981 105981.

Rossignol, C., Lana, C., Alkmim, F., 2020b. Geodynamic evolution of the Minas Basin, southern São Francisco Craton (Brazil), during the early Paleoproterozoic: Climate or tectonic?. J. South Am. Earth Sci. 101,. https://doi.org/10.1016/j.jsames.2020.102628 102628.

Roverato, M., 2016. The Montesbelos mass-flow (southern Amazonian craton, Brazil): a Paleoproterozoic volcanic debris avalanche deposit?. Bull. Volcanol. 78, 1–6. https://doi.org/10.1007/s00445-016-1043-2.

Rubatto, D., 2002. Zircon trace element geochemistry: partitioning with garnet and the link between U-Pb ages and metamorphism. Chem. Geol. 184, 123–138. https://doi.org/10.1016/S0009-2541(01)00355-2.

Salminen, J., Oliveira, E.P., Piispa, E.J., Smirnov, A.V., Trindade, R.I.F., 2019. Revisiting the paleomagnetism of the Neoarchean Uauá mafic dyke swarm, Brazil: Implications for Archean supercratons. Precambrian Res. 329, 108–123. https://doi.org/10.1016/j.precamres.2018.12.001.

Santos, J.O.S., Hartmann, L.A., Gaudette, H.E., Groves, D.I., Mcnaughton, N.J., Fletcher, I.R., 2000. A New Understanding of the Provinces of the Amazon Craton Based on Integration of Field Mapping and U-Pb and Sm-Nd Geochronology. Gondwana Res. 3, 453–488. https://doi.org/10.1016/S1342-937X(05)70755-3.

Santos, M.M., Lana, C., Scholz, R., Buick, I., Schmitz, M.D., Kamo, S.L., Gerdes, A., Corfu, F., Tapster, S., Lancaster, P., Storey, C.D., Basei, M.A.S., Tohver, E., Alkmim, A.R., Nalini, H., Krambrock, K., Fantini, C., Wiedenbeck, M., 2017. A New Appraisal of Sri Lankan BB Zircon as a Reference Material for LA-ICP-MS U-Pb Geochronology and Lu-Hf Isotope Tracing. Geostand. Geoanalytical Res. 41, 335–358. https://doi.org/10.1111/ggr.12167.

Sardinha, A.S., Barros, C.E.M., Krymsky, R., 2006. Geology, geochemistry, and U-Pb geochronology of the Archean (2.74 Ga) Serra do Rabo granite stocks, Carajás Metallogenetic Province, northern Brazil. J. South Am. Earth Sci. 20, 327–339. https://doi.org/10.1016/j.jsames.2005.11.001.

Schofield, D.I., Horstwood, M.S.A., Pitfield, P.E.J., Crowley, Q.G., Wilkinson, A.F., Sidaty, H.C.O., 2006. Timing and kinematics of Eburnean tectonics in the central Reguibat Shield. Mauritania. J. Geol. Soc. London. 163, 549–560. https://doi.org/10.1144/0016-764905-097.

Schröder, S., Bedorf, D., Beukes, N.J., Gutzmer, J., 2011. From BIF to red beds: Sedimentology and sequence stratigraphy of the Paleoproterozoic Koegas Subgroup (South Africa). Sediment. Geol. 236, 25–44. https://doi.org/10.1016/j.sedgeo.2010.11.007.

Shore, M., Fowler, A.D., 1996. Oscillatory zoning in minerals: a common phenomenon. Can. Mineral. 34, 1111–1126.

Siepierski, L., Ferreira Filho, C.F., 2020. Magmatic structure and petrology of the Vermelho Complex, Carajás Mineral Province, Brazil: Evidence for magmatic processes at the lower portion of a mafic-ultramafic intrusion. J. South Am. Earth Sci. 102,. https://doi.org/10.1016/j.jsames.2020.102700 102700.

Siepierski, L., Ferreira Filho, C.F., 2016. Spinifex-textured komatiites in the south border of the Carajas ridge, Selva Greenstone belt, Carajás Province. Brazil. J. South Am. Earth Sci. 66, 41–55. https://doi.org/10.1016/j.jsames.2015.12.011.

Silva, F.F.D., Oliveira, D.C.D., Antonio, P.Y.J., D'Agrella-Filho, M.S., Lamarao, C.N., 2016. Bimodal magmatism of the Tucumã area, Carajás province: U-Pb geochronology, classification and processes. J. South Am. Earth Sci. 72, 95–114. https://doi.org/10.1016/j.jsames.2016.07.016.

Sláma, J., Košler, J., Condon, D.J., Crowley, J.L., Gerdes, A., Hanchar, J.M., Horstwood, M.S.A., Morris, G.A., Nasdala, L., Norberg, N., Schaltegger, U., Schoene, B., Tubrett, M.N., Whitehouse, M.J., 2008. Plešovice zircon — A new natural reference material for U-Pb and Hf isotopic microanalysis. Chem. Geol. 249, 1–35. https://doi.org/10.1016/j.chemgeo.2007.11.005.

Souza, S.R.C., Botelho, N.F., Dantas, E.L., Jiménez, F.A.C., Reis, M.A., Viana, C.S., 2020. Geochemistry and isotopic geology of the Lagoa Seca gold deposit in the Andorinhas greenstone-belt, Carajás Province. Brazil. J. South Am. Earth Sci. 99,. https://doi.org/10.1016/j.jsames.2020.102523 102523.

Spencer, C.J., Kirkland, C.L., Taylor, R.J.M., 2016. Strategies towards statistically robust interpretations of in situ U-Pb zircon geochronology. Geosci. Front. 7, 581–589. https://doi.org/10.1016/j.gsf.2015.11.006.

Tallarico, F.H.B., Figueiredo, B.R., Groves, D.I., Kositcin, N., McNaughton, N.J., Fletcher, I.R., Rego, J.L., 2005. Geology and SHRIMP U-Pb geochronology of the Igarapé Bahia deposit, Carajás copper-gold belt, Brazil: An Archean (2.57 Ga) example of Iron-Oxide Cu-Au-(U-REE) mineralization. Econ. Geol. 100, 7–28. https://doi.org/10.2113/100.1.0007.

Tang, H., Chen, Y., 2013. Global glaciations and atmospheric change at ca. 2.3 Ga. Geosci. Front. 4, 583–596. https://doi.org/10.1016/j.gsf.2013.02.003.

Tassinari, C.C.G., Macambira, M.J.B., 1999. Geochronological provinces of the Amazonian Craton. Episodes 22, 174–182. https://doi.org/10.1080/00206819709465329.

Tavares, F.M., Trouw, R.A.J., da Silva, C.M.G., Justo, A.P., Oliveira, J.K.M., 2018. The multistage tectonic evolution of the northeastern Carajás Province, Amazonian Craton, Brazil: Revealing complex structural patterns. J. South Am. Earth Sci. 88, 238–252. https://doi.org/10.1016/j.jsames.2018.08.024.

Teixeira, J.B.G., Eggler, D.H., 1994. Petrology, geochemistry, and tectonic setting of Archean basaltic and dioritic rocks from the N4 iron deposit, Serra dos Carajás, Pará. Brazil. Acta Geol. Leopoldensia 17, 71–114.

Teixeira, W., Figueiredo, M.C.H., 1991. An outline of Early Proterozoic crustal evolution in the São Francisco craton, Brazil: a review. Precambrian Res. 53, 1–22. https://doi.org/10.1016/0301-9268(91)90003-S.

Teixeira, W., Hamilton, M.A., Girardi, V.A.V., Faleiros, F.M., Ernst, R.E., 2019. U-Pb baddeleyite ages of key dyke swarms in the Amazonian Craton (Carajás/Rio Maria and Rio Apa areas): Tectonic implications for events at 1880, 1110 Ma, 535 Ma and 200 Ma. Precambrian Res. 329, 138–155. https://doi.org/10.1016/j.precamres.2018.02.008.

Tolbert, G.E., Tremaine, J.W., Melcher, G.C., Gomes, C.B., 1971. The Recently Discovered Serra dos Carajás Iron Deposits, northern Brazil. Econ. Geol. 66, 985–994. https://doi.org/https://doi.org/10.2113/gsecongeo.66.7.985.

Toledo, P.I.F., Moreto, C.P.N., Xavier, R.P., Gao, J.F., de Matos, J.H.S.N., de Melo, G.H.C., 2019. Multistage evolution of the Neoarchean (ca. 2.7 Ga) Igarapé cinzento (GT-46) iron oxide copper-gold deposit, Cinzento shear zone, Carajás Province. Brazil. Econ. Geol. 114, 1–34. https://doi.org/10.5382/econgeo.2019.4617.

Trendall, A.F., 2002. The significance of iron-formation in the Precambrian stratigraphic record, in: Altermann, W., Corcoran, P.L. (Eds.), Special Publication of the International Association of Sedimentologists. International Association of Sedimentologists Special Publication, pp. 33–66.

Trendall, A.F., Basei, M.A.S., De Laeter, J.R., Nelson, D.R., 1998. SHRIMP zircon U-Pb constraints on the age of the Carajas formation, Grao Para Group, Amazon Craton. J. South Am. Earth Sci. 11, 265–277. https://doi.org/10.1016/S0895-9811(98)00015-7.

Trunfull, E.F., Hagemann, S., Xavier, R.P., Moreto, C.P.N., 2020. Critical assessment of geochronological data from the Carajás Mineral Province, Brazil: implications for metallogeny and tectonic evolution. Ore Geol. Rev. 103556. https://doi.org/10.1016/j.oregeorev.2020.103556.

Turner, S., Rushmer, T., Reagan, M., Moyen, J.-F., 2014. Heading down early on? Start of subduction on earth. Geology 42, 139–142. https://doi.org/10.1130/G34886.1.

Vasquez, M.L., Rosa-Costa, L.T., 2008. Geologia e recursos minerais do estado do Pará: texto explicativo. CPRM - Serviço Geol. do Bras. 328 (in Portuguese).

Vermeesch, P., 2012. On the visualisation of detrital age distributions. Chem. Geol. 312–313, 190–194. https://doi.org/10.1016/j.chemgeo.2012.04.021.

Villas, R.N., Santos, M.D., 2001. Gold deposits of the Carajás mineral province: Deposit types and metallogenesis. Miner. Depos. 36, 300–331. https://doi.org/10.1007/s001260100178.

Vlaar, N.J., 2000. Continental emergence and growth on a cooling Earth. Tectonophysics 322, 191–202. https://doi.org/10.1016/S0040-1951(00)00063-9.

von Quadt, A., Gallhofer, D., Guillong, M., Peytcheva, I., Waelle, M., Sakata, S., 2014. U-Pb dating of CA/non-CA treated zircons obtained by LA-ICP-MS and CA-TIMS techniques: Impact for their geological interpretation. J. Anal. At. Spectrom. 29, 1618–1629. https://doi.org/10.1039/C4JA00102H.

Windley, B.F., Kusky, T., Polat, A., 2021. Onset of plate tectonics by the Eoarchean. Precambrian Res. 352,. https://doi.org/10.1016/j.precamres.2020.105980 105980.

Wirth, K.R., Gibbs, A.K., Olszewski, W.J., 1986. U-Pb ages of zircons from the Grão-Pará Group and Serra dos Carajás Granites, Pará. Brazil. Rev. Bras. Geociências 16, 195–200.

Young, G.M., 2013. Precambrian supercontinents, glaciations, atmospheric oxygenation, metazoan evolution and an impact that may have changed the second half of Earth history. Geosci. Front. 4, 247–261. https://doi.org/10.1016/j.gsf.2012.07.003.

Vasquez, M.L., Sousa, C.S., Carvalho, J.M.A., 2008. Mapa Geológico do Estado do Pará. Scale 11,000,000 (in Portuguese).